Visualizing Local Vector Field Topology

Gerik Scheuermann
Center for Image Processing and Integrated Computing
Department of Computer Science
University of California
Davis, CA 95616-8562
scheuer@ucdavis.edu

Bernd Hamann
Center for Image Processing and Integrated Computing
Department of Computer Science
University of California
Davis, CA 95616-8562
hamann@cs.ucdavis.edu

Kenneth I. Joy
Center for Image Processing and Integrated Computing
Department of Computer Science
University of California
Davis, CA 95616-8562
joy@cs.ucdavis.edu

Wolfgang Kollmann
Department of Mechanical and Aeronautical Engineering
University of California
Davis, CA 95616
wkollmann@ucdavis.edu

Abstract

The visualization of vector fields has attracted much attention over the last decade due to the vast variety of applications in science and engineering. Topological methods have been used intensively for

global structure extraction and analysis. Recently, there has been a growing interest in local structure analysis due to its connection to automatic feature extraction and speed. We present an algorithm that extracts local topological structure of arbitrary regions in a 2D vector field. It is based on a mathematical analysis of the topological vector field structure in these regions. The algorithm deals with piecewise linear vector fields and arbitrary polygonal regions. We have tested the algorithm for well known analytic vector fields and data sets resulting from computational fluid dynamics.

1. Introduction

Fluid mechanics is a major application for vector field visualization. A velocity field contains the answers to many of the important questions of phycisists and engineers and, due to rotation, the velocity can usually not be described by a gradient field, so an analysis of a single scalar field does not capture the whole structure. Since fluid mechanics is an essential part of the aerospace and automotive industries, there is a strong need for better analysis and visualization methods. Topology has been used in fluid mechanics for several years to interprete experiments and deduct theoretical results, see [4], [5], [19]. These ideas provided the foundation for the use of vector field topology for the analysis and visualization by Helman and Hesselink [10] as well as Globus et al. [8].

Mathematically, vector fields are geometric representations of differential equations, and the number of experimental and numerical data sets defined by discretized vector field is growing rapidly. The analysis and visualization of the resulting data sets still pose challenges to the visualization community. One standard method is based on topological analysis of vector field data, see [10], [8], [28]. These methods require an analysis of the whole vector field to provide answers on the structure, and certain methods may also miss certain features [14]. For this reason, several local analysis algorithms have been developed that are based on topology or related concepts like derivative and eigenvector analysis, see [24], [13].

In this paper, we localize the concept of topology analysis by concentrating on an arbitrary region inside a 2D vector field that we analyze without using information outside the region. It turns out that a

substantial extension of the standard algorithm for topology analysis is necessary to accomplish correct local analysis. Besides the critical points, one has to analyze the boundary of a local region based on *inflow* or *outflow* conditions. This analysis allows us to determine additional separatrices that make, in a topological sense, a separation of the local region into areas of topologically uniform flow possible.

The mathematical background is developed in Sections 2 and 3. Some special cases concerning piecewise linear vector fields are discussed in Section 4. In Section 5, we prove the correctness of the algorithm for several analytical examples. Especially, we highlight the effect of including the boundary of a polygonal region into the analysis of a field. Section 6 shows results for two computational fluid dynamics (CFD) data sets. In Section 7, we provide conclusions and illude to further research.

2. Vector Field Topology

The study of topology of vector fields is based on several basic theorems from the theory of ordinary differential equations, see [1], [9], [11], [16], [22], [23]. We survey the important terms and results for planar, steady vector fields:

Definition 2.1 *A* **planar vector field** *is a map*

$$\begin{aligned} v : \mathbb{R}^2 &\rightarrow \mathbb{R}^2 \,, \\ x &\mapsto v(x) \,. \end{aligned} \tag{1}$$

Usually, one is not so much interested in the vector field per se but in its integral curves:

Definition 2.2 *An* **integral curve through a point** $x \in \mathbb{R}^2$ *of a vector field* $v : \mathbb{R}^2 \rightarrow \mathbb{R}^2$ *is a map*

$$\alpha_x : \mathbb{R} \supset I \rightarrow \mathbb{R}^2 \,, \tag{2}$$

where

$$\alpha_x(0) = x_0 \,, \tag{3}$$

$$\dot{\alpha}_x(t) = v\left(\alpha(t)\right) \,, \qquad \forall\, t \in I \,. \tag{4}$$

Concerning the theorem on existence and uniqueness of integral curves, the *Lipschitz condition* has to be satisfied:

Definition 2.3 *Let $U \subset \mathbb{R}^2$ be an open subset. A continous vector field $v : \mathbb{R}^2 \to \mathbb{R}^2$ satisfies a* **Lipschitz condition on** *U provided there exists a real number $K > 0$ such that*

$$\|Dv(x) - Dv(y)\| \leq K\|x - y\| \tag{5}$$

holds for all $x, y \in U$ and all $t \in J$ where Dv denotes the differential of the vector field v. The constant K is called **Lipschitz constant**.

One can now formulate the existence and uniqueness theorem:

Theorem 2.4 (Existence and uniqueness of integral curves) *Let $v : \mathbb{R}^2 \to \mathbb{R}^2$ be a vector field satisfying the Lipschitz condition on any open neighborhood around point $x \in \mathbb{R}^2$. Then there exists one and only one integral curve through any $x_0 \in \mathbb{R}^2$.*

Proof: See [16, pp. 66–68].

If a vector field satisfies the Lipschitz condition for an open neighborhood of every point, then the integral curves are defined over the whole time line.

Lemma 2.5 *If $v : \mathbb{R}^2 \to \mathbb{R}^2$ is Lipschitz-continous around each point $a \in \mathbb{R}^2$, then every integral curve is defined over the whole time line $\mathbb{R}$.*

Proof: See [16, pp. 90].

This leads to an analysis of the asymptotic behavior of integral curves. The following terms are used to study asymptotic behavior:

Definition 2.6 *Let $v : \mathbb{R}^2 \to \mathbb{R}^2$ be a Lipschitz-continous vector field and $\alpha : \mathbb{R} \to \mathbb{R}^2$ an integral curve. The set*

$$\{a \in \mathbb{R}^2 | \exists (t_n)_{n=0}^{\infty} \subset \mathbb{R}, t_n \to \infty, \lim_{n\to\infty} \alpha(t_n) \to a\} \tag{6}$$

is called ω**-limit set of** α*. The set*

$$\{a \in \mathbb{R}^2 \,|\exists (t_n)_{n=0}^{\infty} \subset \mathbb{R}, t_n \to -\infty, \lim_{n\to\infty} \alpha(t_n) \to a\} \tag{7}$$

is called α**-limit set of** α.

Standard algorithms limit topological analysis to α- and ω-limit sets consisting of critical points.

Definition 2.7 *A* **critical point** *of* $v : \mathbb{R}^2 \to \mathbb{R}^2$ *is a point* $p \in \mathbb{R}^2$ *with* $v(p) = 0$.

Two cases are of interest: (1) sinks and (2) sources.

Definition 2.8 *Let* $v : \mathbb{R}^2 \to \mathbb{R}^2$ *be a Lipschitz-continous vector field,* $z \in \mathbb{R}^2$ *a critical point. If there is a neighborhood* $U \subset \mathbb{R}^2$ *of* z *such that all integral curves in* U *have a* α*-limit set consisting only of* z*, then* z *is called a* **source***. If there is a neighborhood* $U \in \mathbb{R}^2$ *of* z *such that all integral curves in* U *have a* ω*-limit set consisting only of* z*, then* z *is called a* **sink**.

Figure 1 shows a source in the upper part. All integral curves around the critical point start at this critical point. In the lower part, a sink is shown. Every integral curve in the neighborhood ends at the sink. We restrict our consideration further to simple critical points. For the analysis of a vector field, one has to determine the asymptotic behavior of all its integral curves. This is done by analyzing the union of all integral curves starting or ending at the same critical point, called *basin*.

Definition 2.9 *Let* $v : \mathbb{R}^2 \to \mathbb{R}^2$ *be a Lipschitz-continous vector field and* $a \in \mathbb{R}^2$ *a critical point. The union of all integral curves of* v *that converge to* a *for* $t \to -\infty$ *is called* α**-basin of** a*, denoted by* $B_\alpha(a)$*. The union of all integral curves of* v *that converge to* a *for* $t \to \infty$ *is called* ω**-basin of** a*, denoted by* $B_\omega(a)$.

For sinks and sources, one can prove the following lemma:

Lemma 2.10 *Let* v *and* a *be as defined in 2.9. If* a *is a source then* $B_\alpha(a)$ *is an open subset of* $\mathbb{R}^2$*. If* a *is a sink then* $B_\omega(a)$ *is an open subset of* $\mathbb{R}^2$.

Proof: See [11, pp. 181-182].

Figure 2 shows a typical α-basin of a source.

Definition 2.11 *If a subset $S \subset \mathbb{R}^2$ allows a description as a pure n-dimensional manifold, we define the dimension of S as n.*

Remark 2.12 *We need the term dimension only for basins. The previous definition means that an open basin in $\mathbb{R}^2$ is a 2-manifold, a basin consisting of a finite number of stream lines is a 1-manifold and a basin consisting of a finite number of points is a 0-manifold.*

If all limit sets are critical points and one regards infinity as an additional critical point, then the whole plane is separated into basins of sources, sinks and infinity. The boundaries of open basins cannot belong to the basins themselves. Since there are no other possibilities, the boundaries start at the remaining critical points or at infinity. With the assumption that all critical points are simple, these remaining critical points are saddle points.

Theorem 2.13 *Let $v : \mathbb{R}^2 \to \mathbb{R}^2$ be a Lipschitz-continous vector field. Let all α- and ω-limit sets be simple critical points and ∞. Let $a_1, \ldots, a_j$ be the sources, $s_1, \ldots, s_k$ be the saddles, and $z_1, \ldots, z_m$ be the sinks. Then $\mathbb{R}^2$ can be divided into disjoint α-basins,*

$$\mathbb{R}^2 = \bigcup_{i=1}^{j} B_\alpha(a_i) \cup \bigcup_{i=1}^{k} B_\alpha(s_i) \cup \bigcup_{i=1}^{l} \{z_i\} \cup B_\alpha(\infty)\,. \tag{8}$$

It can also be divided into disjoint ω-basins,

$$\mathbb{R}^2 = \bigcup_{i=1}^{l} B_\omega(z_i) \cup \bigcup_{i=1}^{k} B_\omega(s_i) \cup \bigcup_{i=1}^{j} \{a_i\} \cup B_\omega(\infty)\,. \tag{9}$$

Proof: Every point belongs to exactly one stream line. By the assumption, the stream line has to start at one of the critical points or at the boundary, so it is in one of the basins. This gives the first partition. The second partition is given by a look at the end of a stream line. $\diamond$

The topological structure is given by all intersections between α- and ω-basins. The description of these intersections uses the dimension of the different basins. The α-basins of the sources and the ω-basins

of the sinks alone can contain open subsets besides the basins of infinity. It follows from Lemma 2.10 that their intersections form 2D (open) "faces" of the structure. The boundaries do not belong to these basins and consist of curves and points. A curve can only be part of a basin of a saddle. The method by Helman et al. [10] uses this fact to determine the structure by finding all critical points and then drawing all basins of the saddles. Apart from the critical points, the resulting plane consists of faces of the resulting graph, sometimes called "topological skeleton." These faces are the intersections between the α-basins of the sources and the ω-basins of the sinks. It can be shown that they can be deformed into a topologically uniform flow. This provides the mathematical explanation for the description of the whole process as separating the vector field into *domains of topologically uniform flow*.

3. Local vector field topology

In most practical applications, the domain of a vector field is finite. It is usually either the union of all the cells of a finite-element or finite-difference grid or the convex hull of scattered data points without connectivity. Topologically, this means that a vector field is defined over a closed and bounded, i.e., compact, subset of the real plane. The analysis of a vector field should reflect this property. However, current visualization algorithms used to date do not do this. The main reason for this is the fact that standard algorithms operate on the whole domain of a vector field, and the flow is typically very simple on the boundaries. The boundary is either a solid boundary, where the flow is set to tangential flow (often zero), or it is an open boundary, where the flow has a simple structure. In a wind tunnel experiment, for example, there is one inflow region and one outflow region. We, by contrast, want to analyze an arbitrary compact region inside the domain of a vector field. We will show that one has to analyze the boundary completely to obtain a correct analysis. For this purpose, we generalize some of the terms of the last section. This explains also some possible structures at infinity, since infinity plays the role of the boundary.

The first change concerns Lemma 2.5. Since we must consider a boundary now, an integral curve in a Lipschitz-continuous, steady vector field might start or end on the boundary. One might imagine a vector field over the whole plane with a compact region cut out of it resulting in the given vector field.

The integral curves are also cut; they still can be continued inside the local region, but they may end or start on the boundary.

Lemma 3.1 *Let $D \subset \mathbb{R}^2$ be a compact subset and $v : D \to \mathbb{R}^2$ be a Lipschitz-continous vector field. Then, for an arbitrary integral curve $\alpha : (a, b) \to D$ of maximal length, a will be finite only if $\alpha(a) \in \partial D$, where ∂D denotes the boundary of D. Analogously, b will be finite only if $\alpha(b) \in \partial D$.*

Since we want to establish a theorem similar to Theorem 2.13, we distinguish three subsets of the boundary with respect to the vector field. These three subsets are the sets of inflow, outflow, and boundary flow points. The connected components of the inflow and outflow regions play the role of additional sources and sinks in the topological analysis. The end points lead to the additional separatrices that would be missed when using the standard approach.

Definition 3.2 *Let $D \subset \mathbb{R}^2$ be a compact domain of a Lipschitz-continous vector field $v : D \to \mathbb{R}^2$. Let $d \in \partial D$ be a point on the boundary. We define the following three entities:*

(1) The point d is called an **outflow point** *if every integral curve through d ends at d and there exists an integral curve through d that does not contain another point of ∂D. The set of all outflow points is called* **outflow set**.

(2) The point d is called a **inflow point** *if every integral curve through d starts at d and there exists an integral curve through d that does not contain another point of ∂D. The set of all inflow points is called* **inflow set**.

(3) The point d is called a **boundary flow point** *if there exists an integral curve $\alpha_d : (-\epsilon, \epsilon) \to D$, $\epsilon > 0$, through d lying completely inside ∂D. The set of all boundary flow points is called* **boundary flow set**.

The topological situations around an outflow point, an inflow point and a boundary flow point are sketched in Figure 3. In most practical applications, the vector field has a piecewise linear boundary. This case will be handled explicitly in Section 4. The inflow and outflow regions play the role of sinks and sources.

Lemma 3.3 *Let I_i be a connected component of the inflow set I. The α-basin $B_\alpha(I_i)$ is the union of all integral curves starting inside I_i. This basin is open. Let O_i be a connected component of the inflow set $O \subset \partial D$. The ω-basin $B_\omega(O_i)$ is the union of all integral curves ending inside O_i. This basin is also open.*

Proof: The sets are open due to the continuity of the solution of the initial value problem with respect to parameters like the starting point. If a point is in a small neighborhood of a curve in the basin, then its corresponding integral curve is close to this curve at another point. Since our basins are created by open subsets of the boundary, they are themselves open in D. $\diamond$

A boundary of an open basin cannot belong to the basin; thus, it must start at the boundary points between the inflow and outflow sets. We call these starting points **boundary saddles** to reflect the similarity to the saddle points inside the domain.

Definition 3.4 *Let $D \subset \mathbb{R}^2$ be a compact subset with a smooth boundary. Let $v : D \to \mathbb{R}^2$ be a Lipschitz-continous vector field. A point $d \in \partial D$ that is no inflow, outflow, or boundary flow point is called* **boundary saddle**.

It is now possible to describe D as a union of disjoint topologically uniform flow regions:

Theorem 3.5 *Let $D \subset \mathbb{R}^2$ be a compact subset with a smooth boundary. Let $v : D \to \mathbb{R}^2$ be a Lipschitz-continous vector field. Let $a_1, \ldots, a_j$ be the sources, $s_1, \ldots, s_k$ be the saddles, $b_1, \ldots, b_p$ be the boundary saddles, and $z_1, \ldots, z_l$ be the sinks. Furthermore, let $I_1, \ldots, I_m$ be the inflow components, and $O_1, \ldots, O_n$ be the outflow components. If we assume that there are no other α- and ω-limit sets, then D can be divided into α-basins,*

$$D = \bigcup_{i=1}^{j} B_\alpha(a_i) \cup \bigcup_{i=1}^{m} B_\alpha(I_i) \cup \bigcup_{i=1}^{l} B_\alpha(s_i) \cup \bigcup_{i=1}^{p} B_\alpha(b_i) \cup \bigcup_{i=1}^{n} O_i \cup \bigcup_{i=1}^{k} \{z_i\} \,. \tag{10}$$

The region D can also be divided into ω-basins,

$$D = \bigcup_{i=1}^{k} B_\omega(z_i) \cup \bigcup_{i=1}^{n} B_\omega(O_i) \cup \bigcup_{i=1}^{l} B_\omega(s_i) \cup \bigcup_{i=1}^{p} B_\omega(b_i) \cup \bigcup_{i=1}^{m} I_i \cup \bigcup_{i=1}^{j} \{a_i\} \,. \tag{11}$$

Proof: Every point belongs to exactly one stream line. This stream line has to start at a critical point, i.e. a source, sink or saddle, or at the boundary, i.e., an inflow region, an outflow region or a boundary saddle, since we excluded other α-limit sets. This shows the first partition. The same argument for the ending of stream lines shows the second partition. $\diamond$

Both parts of the theorem are illustrated in Figure 4. In the upper part, the figure shows a decomposition of a vector field into α-basins. In the center, it shows the decomposition of the same vector field into ω-basins. We are interested in the connected components of the intersections between α- and ω-basins. Since these components consist of integral curves starting at a connected part of the boundary (or a critical point inside the domain) and ending at a specific connected part of the boundary (or a critical point inside the domain), one can transform the whole region into topologically uniform flow. Thus, one can separate the vector field into regions of topologically uniform flow. The 2D intersections are built by intersections of α-basins of sources or α-basins of inflow regions with ω-basins of sinks or ω-basins of outflow regions. The boundaries of these regions consist of the critical points, the boundary saddles, the basins of the saddles, and connected subsets of boundary flow points. The lower part of Figure 4 shows the decomposition into these intersections for the simple vector field used above. One can describe the topological structure of the vector field by drawing the critical points, boundary saddles and the integral curves starting or ending at the saddles and boundary saddles. In the figure, the information about the vector field structure can be given by the red, blue and green elements.

4. Linear local vector field topology

This section deals with the specific cases to be considered for a piecewise linear vector field defined over a triangulation in the plane. This case will occur in all the examples shown in Sections 5 and 6. The changes and additions to the previous section deal with the situation on the boundary. One has to deal with the vertices of a polygon, i.e., the boundary is not a smooth curve. We use scalar products of the vector field at certain positions and outward normals of the boundary edges to analyze the vector field. Together with the procedure from [10], one can construct an algorithm extracting the local topology.

We assume that the domain D is triangulated and that the vector field is defined by piecewise linear

interpolation of vectors at the vertices of the triangulation. The analysis of the local vector field topology is simplified on the boundary by performing linear interpolation along the edges. For interior points of the edges, we use Lemma 4.1:

Lemma 4.1 *Let $D \subset \mathbb{R}^2$ be a triangulated 2D-domain and ∂D be its polygonal boundary consisting of one or more polygons. Let $v : D \to \mathbb{R}^2$ be a piecewise linear vector field defined over the triangulation of D. Let $d \in \partial D$ be an interior point on a boundary edge e and $n \in \mathbb{R}^2$ be the outward normal of the edge. There are four possibilities:*

(1) If $v(d) \cdot n > 0$ holds, d is an outflow point.

(2) If $v(d) \cdot n < 0$ holds, d is an inflow point.

(3) If $v(d) \cdot n = 0$ holds and d is the only point for which this condition holds on the edge, d is a boundary saddle. (The integral curve through d is a separatrix, and one has to integrate it in negative and positive temporal directions.)

(4) If $v(d) \cdot n = 0$ holds for all points on the edge, then d is a boundary flow point.

Proof: Let $x \in D$ be any point. The above four statements are true because $v(x) \cdot n = 0$ is a linear condition along the edge, since

$$v(x) = (1-t)v_0 + tv_1\,, \tag{12}$$

where

$$x = (1-t)p_0 + tp_1\,, \tag{13}$$

where p_0 and p_1 denote the end points of the edge and v_0 and v_1 the vector values at these positions. It follows that

$$v(x) \cdot n = (1-t)v_0 \cdot n + tv_1 \cdot n\,, \tag{14}$$

which is a simple linear equation that can be either zero at one point or at all points. If $v(x) \cdot n$ is zero at all points, then the flow stays on the edge, proving (4). If $v(x) \cdot n$ is zero at only one point, then $v(x) \cdot n$ is positive on one side and negative on the other side of d, which implies that d is a boundary saddle

since the integral curve "touches" the edge at that point (or contains just that point). The first two cases imply that the integral curve ends or starts at d, and, due to continuity, the integral curve leads into the interior of D or originates from there. $\diamond$

For the analysis of an endpoint p on a boundary edge, one has to check the vector field value with the normals m and n of the two adjacent boundary edges. One has to distinguish the convex, collinear, and concave cases. The analysis is always based on the behavior of the vector field on two consecutive boundary edges. If the vector at the vertex under consideration is not tangential to one of the edges, one can determine the type of the vertex by calculating the scalar products $m \cdot v(p)$ and $n \cdot v(p)$ of the vector at the vertex with the two outward normals of the edges. This defines the topological behavior of the vector field in a neighborhood of the vertex on the boundary. If the field is tangential to one edge (or both, in the collinear case), one has to analyze the vector at the other end of the edge(s) to determine the topological type of the vertex with respect to the vector field. We formulate three Lemmata to describe all possible cases and illustrate the situations in Figures 5-7. The algorithm uses these properties to find the boundary saddles and the separatrices starting from there. The first Lemma deals with the convex case:

Lemma 4.2 *Let p be a convex boundary vertex of D, and let m and n be the normals of the two adjacent boundary edges. Furthermore, let o and q be the endpoints of the two boundary edges. We distinguish five cases:*

(A1) If $(v(p) \cdot m)\,(v(p) \cdot n) < 0$ holds, then the integral curve through p in D contains only p.

(A2) If $(v(p) \cdot m)\,(v(p) \cdot n) > 0$ holds, then p is an outflow or inflow point, depending on the common sign of the products.

(A3) If $v(p) \cdot m = 0$ and $v(o) \cdot m > 0$ holds, then p is a outflow point.

(A4) If $v(p) \cdot m = 0$ and $v(o) \cdot m = 0$ holds, then p is a boundary saddle. (The integral curve through p stays on the first edge and leaves D at p, so one does not have a separatrix entering the interior of D at p.)

(A5) If $v(p) \cdot m = 0$ and $(v(o) \cdot m) < 0$ hold, then p is a boundary saddle. (The integral curve through p consists only of p, so one has no separatrix entering the interior of D at p.)

An analysis of the cases with $v(p) \cdot n = 0$ yields the same results.

Proof: The typical situation $(v(p) \cdot m)\,(v(p) \cdot n) < 0$ is shown in the upper-left corner of Figure 5. The vector and its inverse lead out of D such that the integral curve consists only of p. Concerning case (A2), the vector field points either outward at p (and in a neighborhood on both edges) or inward on a complete boundary neighborhood, as shown in the upper-right corner of Figure 5. Then, p is an ordinary outflow or inflow point. Case (A3) is shown in the left-middle image of Figure 5. The point p is in the middle of an outflow region; therefore, it is an outflow point. In case (A4), the integral curve through p stays on the edge from o to p and leaves D there, as can be seen in the right-middle image of Figure 5. Finally, case (A5) is shown in the lower-left corner of Figure 5. All integral curves in a neighborhood of p enter D on one edge and leave it on the other. Thus, so that the integral curve through p consists only of p itself. $\diamond$

This proves that one does not need to calculate any separatrices in this case. The collinear case is treated in the next lemma:

Lemma 4.3 *Let p be a shared boundary vertex of two collinear edges, and let $v(p) \neq 0$. Furthermore, let $n \in \mathbb{R}^2$ be the outward normal of both edges and o, q the other two endpoints of the edges. One can distinguish eight cases:*

(B1) If $v(p) \cdot n > 0$ holds, then p is an outflow point.

(B2) If $v(p) \cdot n < 0$ holds, then p is an inflow point.

(B3) If $v(p) \cdot n = 0$, $v(o) \cdot n = 0$, and $v(q) \cdot n < 0$ holds, then p is a boundary saddle. (The integral curve through p is a separatrix, and one needs to calculate the part entering the interior of D.)

(B4) If $v(p) \cdot n = 0$, $v(o) \cdot n = 0$, and $v(q) \cdot n = 0$ holds, then the integral curve through p stays on the boundary around p.

(B5) If $v(p) \cdot n = 0$ holds, then $v(o) \cdot n = 0$ and $v(q) \cdot n > 0$ holds, p is a boundary saddle. (The integral curve through p stays on one edge and ends at p. One does not have to calculate a separatrix.)

(B6) If $v(p) \cdot n = 0$ and $((v(o) \cdot n) (v(q) \cdot n)) > 0$ holds, p is an outflow or inflow point, depending on the common sign of the scalar products.

(B7) If $v(p) \cdot n = 0$ and $((v(o) \cdot n) (v(q) \cdot n)) < 0$ holds and $v(x) \cdot n$ changes from outflow to inflow in the direction of the tangential component for points x on the two edges, p is a boundary saddle. (The integral curve through p is a separatrix touching the boundary. One has to integrate it backward and forward in time.)

(B8) If $v(p) \cdot n = 0$ and $((v(o) \cdot n) (v(q) \cdot n)) < 0$ holds and $v(x) \cdot n$ changes from inflow to outflow in the direction of the tangential component for points x on the two edges, the integration curve through p consists only of p.

The remaining cases, where $v(q) \cdot n = 0$, are equivalent to cases (B3) and (B5).

Proof: We use figures to explain the arguments. The upper-left corner of Figure 6 shows the situation in case (B1) and the upper-right corner the situation in case (B2). These cases are equivalent to the standard case inside an edge in Lemma 4.1. In left of the second row of Figure 6, it can be seen that in case (B3) the integral curves lead into the inner part of D at p, wherease the obvious Case (B4) is on the right of the second row. Case (B5) is shown in left of the third row in Figure 6. The integral curve through p ends at p, since there is an outflow region inside the second edge. The right of the third row in Figure 6 shows the integral curves around p in case (B6) with outflow. One can see that the flow can be transformed into topologically uniform outflow. Reversing all vectors yields the inflow case. Case (B7) is shown in the lower-left corner of Figure 6. One integral curve touches p. Thus, three different parts of the flow are visible: One part leaves D, one part enters D, and one part stays inside D. There are two separatrices starting at p, similar to the standard case of a boundary saddle lying in the interior of an edge. Finally, the lower-right corner of Figure 6 shows case (B8). The flow enters on one side of p and

leaves on the other side. Thus, the integral curve through p consists only of p, and there is no separatrix to be calculated. $\diamond$

The remaining case deals with a concave vertex. Lemma 4.4 summarizes the possible patterns:

Lemma 4.4 *Let p be a concave boundary vertex and let m and n be the outward normals of the two edges. Furthermore, let o be the second endpoint of one of the edge with normal m. There are five cases one can consider.*

(C1) If $((v(p) \cdot m)\,(v(p) \cdot n)) > 0$ holds, then p is either an outflow or an inflow point, depending on the common sign of the products.

(C2) If $((v(p) \cdot m)\,(v(p) \cdot n)) < 0$ holds, then p is a boundary saddle. (The integral curve through p is a separatrix that has to be integrated backward and forward in time.)

(C3) If $v(p) \cdot m = 0$ and $v(o) \cdot m > 0$ holds, then the integral curve through p is a separatrix that has to be integrated backward and forward in time.

(C4) If $v(p) \cdot m = 0$ and $v(o) \cdot m < 0$ holds, then p is an inflow point.

(C5) If $v(p) \cdot m = 0$ and $v(o) \cdot m = 0$ holds, then the integral curve through p stays on one edge and enters the interior of D at p, so one has to calculate one part of the curve. (The orientation of the curve is positive, provided the tangential part of $v(p)$ with respect to m is directed into the interior of D. Otherwise, one has to integrate backwards in time.)

An analysis of the cases where $v(p) \cdot n = 0$ holds yields the same results.

Proof: The upper-left corner of Figure 7 shows a typical situation for case (C1), with outflow around p. By reversing all vectors and curve orientations, one obtains the inflow for negative scalar products. Case (C2) is described in the upper-right corner of Figure 7. One can see the integral curve touching the boundary at p. This is the situation on the other side of the boundary of case (A1). The flow is separated at p into an outflow region along on edge, an inflow region along the other edge, and a region of flow staying inside D below the integral curve through p. The case (C3) is shown in the left-middle image of

Figure 7. The topological situation equals (C2), so one obtains the same result. Case (C4) is shown in the right-middle image of Figure 7. The integral curves starting at the boundary around p all enter the interior of D, so one has an inflow point. Finally, in case (C5), the integral curve through p stays on one edge and enters the interior of D at p, so one has to calculate the part of this integral curve inside the interior of D. This is shown in the lower left corner of Figure 7. $\diamond$

These various case distinctions allow us to establish an algorithm to extract local topology: We determine for all critical points in the domain and classify them into sources, sinks, and saddles; then, we analyze all the edges and vertices on all boundaries identifying boundary saddles and separatrices starting there. The next section provides examples.

5. Examples

The theoretical considerations from the last sections aim at an analysis of vector field topology including the boundary. The first examples provided in this section show the effect of this analysis on the understanding of topological vector field structure. They are based on the study of vector fields given by polynomial equations. The construction of these fields is based on considerations based on *Clifford algebra*, see [27], [26]. We briefly review the main topological properties discussed in [27], [26]. Figures 8-13 show unit vectors to indicate the orientation of separatrices and integration curves. Critical points are red, green or blue. Red color indicates a saddle point; green color a source; and blue color a sink. The separatrices are drawn in blue; integral curves are violett; and the boundaries of regions and domains are white..

We start with a vector field containing two sinks and two sources in a rectangular area. The conventional analysis, based on the separatrices starting at saddle points alone, will find no separating curves at all, so the user is left with the question of how the two sources and sinks interact. This can be seen in Figure 8. Since there exist integral curves from one source to both sinks and also to the boundary, not all integration curves belong to the same open basin. We know that, as a result of the piecewise linear interpolation and the analytic structure of the original field, there are no addional critical points or more complicated structures involved in this example. The solution follows as a result of Sections 3 and 4.

There are ten boundary saddles where the flow turns from inflow to outflow. By starting separatrices at these positions it is possible to determine the structure of the flow. The result is shown in Figure 9. The whole rectangle is now divided into open basins with the same α- and ω-basin. Every integral curve in one of these basins starts and ends at the same critical point or connected component of the boundary. It is now easy to understand the interaction of the sinks and sources.

As mentioned before, this example was constructed using an analytic field description. The structure of the entire field is shown in Figure 10. The small white box marks the domain of our example. There are three saddle points where 12 separatrices start. The importance of the saddles for the standard analysis is seen by comparing the result inside the rectangle with the result shown in Figure 8.

Our next example involves two sources and a saddle point on a plane segment. The simple structure is shown together with some integral curves in Figure 11. If one cuts out a rectangular area containing the saddle point, one will miss all the separatrices starting at the saddle point. Performing local topology analysis, however, it is possible to analyze the field, correctly, see Figure 12. There are three boundary saddles: One is inside an edge, and the other two are on concave corners, see Section 4. These separatrices replace the separatrices starting at the saddle point in the global topology shown in Figure 11. They assure the separation of the basins of the two sources and the basins of the inflow regions on the boundary. There are obvious differences between the global and local topology. For comparison, we show all separatrices and integral curves together in Figure 13. It can be seen that the separatrices starting on the boundary are strongly influenced by the placement of the boundary but also by the existence of the saddle point in the overall vector field.

6. Application

We have applied the local topology extraction to a vortex breakdown simulation. Vortex breakdown is a phenomenon observed in a variety of flows ranging from tornadoes to wing tip vortices (Lambourne and Bryer [15]), pipe flows (Sarpkaya[25], Faler and Leibovich[7], Leibovich[17], Lopez[20], [21]) and swirling jets (Billant et al.[2]). The latter flow are important to combustion applications where they are able to create recirculation zones with sufficient residence time for the reactions to approach

completion. The numerical simulation of this type of flow requires an accurate method for the solution of the initial/boundary value problem of the Navier-Stokes equations. The incompressible Navier-Stokes equations are set up for this purpose in cylindrical domains, which may be bounded or unbounded. Analytic mappings are applied to the radial and axial directions to map the physical domain onto the unit cylinder and to control the distribution of grid points. Cylindrical coordinates are well suited for this geometry since they allow Fourier decomposition with respect to the azimuthal direction. However, the metric coefficients produce singularities at the coordinate axis which must be carefully analyzed (Eisen et al.[6]) to ensure stability and accuracy for the simulation of 3D flows. It can be shown that the azimuthal Fourier modes of scalar, vector and tensor variables possess well defined symmetry properties with respect to the radial coordinate and satisfy radial growth laws near the axis depending on the wavenumber. A hybrid spectral finite-difference method (Canuto et al.[3]) based on stream functions for the azimuthal Fourier modes is used for the simulations. The solver allows the choice of second to eighth order for first and second derivatives as explicit central difference operators (Kennedy and Carpenter [12]) or third to ninth order upwind-biased differences (Li [18]). High order filters are used to provide the numerical dissipation to stabilize the system if central difference operators are applied to the convective terms (Kennedy and Carpenter [12]). Runge-Kutta-type time integration methods with minimal storage requirements (Williamson [29], Kennedy and Carpenter [12]) were implemented and the third and fourth order version are currently available in the solver. The Navier-Stokes solver is applied to the vortex breakdown in incompressible jet flows with supercritical swirl numbers (Billant et al. [2]), and the results are used for the topological analysis presented in the previous sections.

The boundary conditions at the nozzle entrance section were determined in accordance with the experiments of Billant et al. [2]. They measured the axial and azimuthal velocities at $z_0/D = 0.6$ ($D = 2R$), which show a distinct dependence on the swirl number S. The simulations were performed for various values of the Reynolds and swirl numbers and the experimental profiles at $z/D = 0.6$ were used as boundary conditions. The image domain was discretized with $n_r \times n_z = 95 \times 251$ grid points, and the third-order accurate minimal storage Runge-Kutta scheme (9) of Williamson [29] was used for time integration. The Reynolds number was $Re = 3000$ and the swirl number $S = 1.25$. The initial condi-

tions were generated by extending the entrance profiles throughout the flow field. Disturbances for the axial velocity and azimuthal vorticity of the order of 0.1 percent were added at the entrance to trigger the Kelvin-Helmholtz instability of the shear layer. The results used for the topological analysis were taken at the dimensionless time $t = 40.989$. The vector field is shown in Figure 14. There are 39909 data points and 79000 triangles in this data set. The piecewise linear interpolation contains 703 simple critical points, creating a complex global topology. The jet enters the domain in the middle of the right boundary.

First, we used a rectangle, shown in Figure 15. The data in this rectangle was used to analyze the local topology. We extract all the critical points and find all the boundary saddles by analyzing the boundary of the rectangle. This resulted in the topological structure shown in Figure 16. One can see some of the additional separatrices starting at the boundary saddles. They separate regions of flow staying inside the boundary from outflow and inflow parts. No analysis of data outside the rectangle has been used. The required computing time does only depend on the size of the region and is (nearly) independent of the size of the overall data set.

It is possible to use multiple regions of interest in the same data set that can be analyzed independently. One may also use arbitrary polygons as boundaries. This is demonstrated in our second analysis of the same jet data set for which we chose three regions, as shown in Figure 17. One region covers a part of the backstream besides the main inflow jet. The second region shows a part of the rectangle we used before. Neither of these two regions contains critical points, which documents the necessity of boundary analysis. The third region shows the mixing process of the jet and the fluid downstream. Figure 18 shows the first two regions in more detail. One can see clearly forward- and backward-facing flow. Without an analysis of the boundary, one obtains no separatrices due to the lack of critical points inside the two regions. The third region is shown in more detail in Figure 19. Since the analysis is limited to a rather small area, it can be analyzed quickly. In the figure, one can spot several separatrices spiraling around critical points. The critical points inside these areas have Jacobians with complex conjugate eigenvalues, thus there are spirals; the real parts of the eigenvalues may have small absolute values, and a stream line in the neighborhood of the critical points approaches them very slowly. Closed stream lines might be

present.

7. Conclusions and Future Work

We have presented a method to analyze the local topology of arbitrary regions in 2D vector fields. Our idea is based on an extraction of the critical points in the domain and an examination of the region's boundary. By determining the inflow, outflow, and boundary flow segments one can separate the domain into regions of topologically uniform flow. A detailed analysis of the possible cases in a piecewise linear flow allows local structure extraction for analytical and gridded data sets. We have outlined the differences to the global topology algorithm in theory and applications, demonstrating the relevance of our localized approach when applied to regions with complicated flow patterns on the boundary. This case is typical for most interesting regions inside a larger data set. Another important situation that we studied is the absence of critical points in a region that provides interesting structure, like backward facing flow. Our algorithm detects these areas and separates them from other parts of the flow leading to better visualizations of local flow structure. Since the local topology analysis does not use any information outside a region of interest, it is very attractive when analyzing large data sets locally and thus reducing computing time significantly.

We plan to extend our ideas to vector fields defined over 3D domains. We will also apply our algorithm to other data sets to gain a deeper understanding of the relation between local and global topology. Besides 3D domains, an analysis of time-dependent simulations is one final goal. The analysis in this paper is linited so far to steady flow, since pathlines will cross each other, especially in a turbulent flow like our application. New ideas are needed to accomplish an analysis over time, but we believe that topology provides a framework to find new ways for analysis and visualization.

8. Acknowledgments

This work was supported by the National Science Foundation under contracts ACI 9624034 and ACI 9983641 (CAREER Awards), through the Large Scientific and Software Data Set Visualization (LSSDSV) program under contract ACI 9982251, and through the National Partnership for Advanced Com-

putational Infrastructure (NPACI); the Office of Naval Research under contract N00014-97-1-0222; the Army Research Office under contract ARO 36598-MA-RIP; the NASA Ames Research Center through an NRA award under contract NAG2-1216; the Lawrence Livermore National Laboratory under ASCI ASAP Level-2 Memorandum Agreement B347878 and under Memorandum Agreement B503159;

and the North Atlantic Treaty Organization (NATO) under contract CRG.971628 awarded to the University of California, Davis. We also acknowledge the support of ALSTOM Schilling Robotics, Chevron, General Atomics, Silicon Graphics, and ST Microelectronics, Inc. We thank the members of the Visualization Group at the Center for Image Processing and Integrated Computing (CIPIC) at the University of California, Davis.

References

[1] V. I. Arnold. *Ordinary Differential Equations.* Springer-Verlag, Berlin, 1992.

[2] P. Billant, J. Chomaz, and P. Huerre. Experimental Study of Vortex Breakdown in Swirling Jets. *Journal of Fluid Mechanics*, 376:183 – 219, 1999.

[3] C. Canuto, M. Y. Hussaini, and T. A. Zang. *Spectral Methods in Fluid Dynamics.* Springer-Verlag, Berlin, 1988.

[4] M. S. Chong, A. E. Perry, and B. J. Cantwell. A General Classification of Three-Dimensional Flow Fields. *Physics of Fluids A*, 2(5):765 – 777, 1980.

[5] U. Dallmann. Topological Structures of Three-Dimensional Flow Separations. Technical Report 221-82 A 07, Deutsche Forschungs- und Versuchsanstalt fuer Luft- und Raumfahrt, 1983.

[6] H. Eisen, W. Heinrichs, and K. Witsch. Spectral Collocation Methods and Polar Coordinate Singularities. *Journal of Computational Physics*, 96:241 – 251, 1991.

[7] J. H. Faler and S. Leibovich. Disrupted States of Vortex Flow and Vortex Breakdown. *Physics of Fluids*, 96:1385 – 1400, 1977.

[8] A. Globus, C. Levit, and T. Lasinski. A Tool for Visualizing the Topology of Three-Dimensional Vector Fields. In *IEEE Visualization '91*, pages 33 – 40, San Diego, 1991.

[9] J. Guckenheimer and P. Holmes. *Dynamical Systems and Bifurcation of Vector Fields.* Springer, New York, 1983.

[10] J. L. Helman and L. Hesselink. Surface Representations of Two- and Three-Dimensional Fluid Flow Topology. In G. M. Nielson and B. Shriver, editors, *Visualization in scientific computing*, pages 6–13, Los Alamitos, CA, 1990.

[11] M. W. Hirsch and S. Smale. *Differential Equations, Dynamical Systems and Linear Algebra*. Academic Press, New York, 1974.

[12] C. A. Kennedy and M. H. Carpenter. Several new Numerical Methods for Compressible Shear Layer Simulations. *Applications of Numerical Mathematics*, 14:397 – 433, 1994.

[13] D. N. Kenwright. Automatic Detection of Open and Closed Separation and Attachment Lines. In D. Ebert, H. Rushmeier, and H. Hagen, editors, *IEEE Visualization '98*, pages 151–158, Los Alamitos, CA, 1998.

[14] D. N. Kenwright, C. Heinze, and C. Levit. Feature Extraction of Separation and Attachment Lines. *IEEE Transactions on Visualization and Computer Graphics*, 5(2):135–144, April–June 1999.

[15] N. C. Lambourne and D. W. Bryer. The Bursting of Leading Edge Vortices: Some Observations and Discussion of the Phenomenon. *Aeronautical Research Council R. & M.*, 3282:1 – 36, 1961.
[16] S. Lang. *Differential and Riemannian Manifolds.* Springer, New York, third edition, 1995.
[17] S. Leibovich. Vortex Stability and Breakdown: Survey and Extension. *AIAA Journal*, 22:1192 – 1206, 1984.
[18] Y. Li. Wavenumber Extended High-Order Upwind-Biased Finite Difference Schemes for Convective Scalar Transport. *Journal of Computational Physics*, 133:235 – 255, 1997.
[19] M. J. Lighthill. Attachment and Separation in Three Dimensional Flow. In R. L., editor, *Laminar Boundary Layers II*, pages 72 – 82. Oxford University Press, Oxford, 1963.
[20] J. M. Lopez. Axisymmetric Vortex Breakdown. part 1. confined Swirling Flow. *Journal of Fluid Mechanics*, 221:533 – 552, 1990.
[21] J. M. Lopez. On the Bifurcation Structure of Axisymmetric Vortex Breakdown in a Constricted Pipe. *Physics of Fluids*, 6:3683 – 3693, 1994.
[22] J. W. Milnor. *Topology from the Differential Viewpoint.* The University Press of Virginia, Charlottesville, 1965.
[23] H. Poincaré. *Mémoire sur les cóurbes définés par les équations différentielles I-IV*. Gauthier-Villar, Paris, 1880-1890.
[24] M. Roth and R. Peikert. A Higher-Order Method for Finding Vortex Core Lines. In *IEEE Visualization '98*, pages 143–150, Los Alamitos, 1998.
[25] T. Sarpkaya. On Stationary and Travelling Vortex Breakdown. *Journal of Fluid Mechanics*, 45:545 – 559, 1971.
[26] G. Scheuermann. *Topological Vector Field Visualization with Clifford Algebra*. PhD thesis, University of Kaiserslautern, Kaiserslautern, Germany, 1999.
[27] G. Scheuermann, H. Hagen, and H. Krüger. An Interesting Class of Polynomial Vector Fields. In M. Dæhlen, T. Lyche, and L. L. Schumaker, editors, *Mathematical Methods for Curves and Surfaces II*, pages 429–436, Nashville, 1998.
[28] G. Scheuermann, H. Krüger, M. Menzel, and A. Rockwood. Visualizing Nonlinear Vector Field Topology. *IEEE Transactions on Visualization and Computer Graphics*, 4(2):109–116, April–June 1998.
[29] J. H. Williamson. Low-Storage Runge-Kutta Schemes. *Journal of Computational Physics*, 35:48 – 56, 1980.

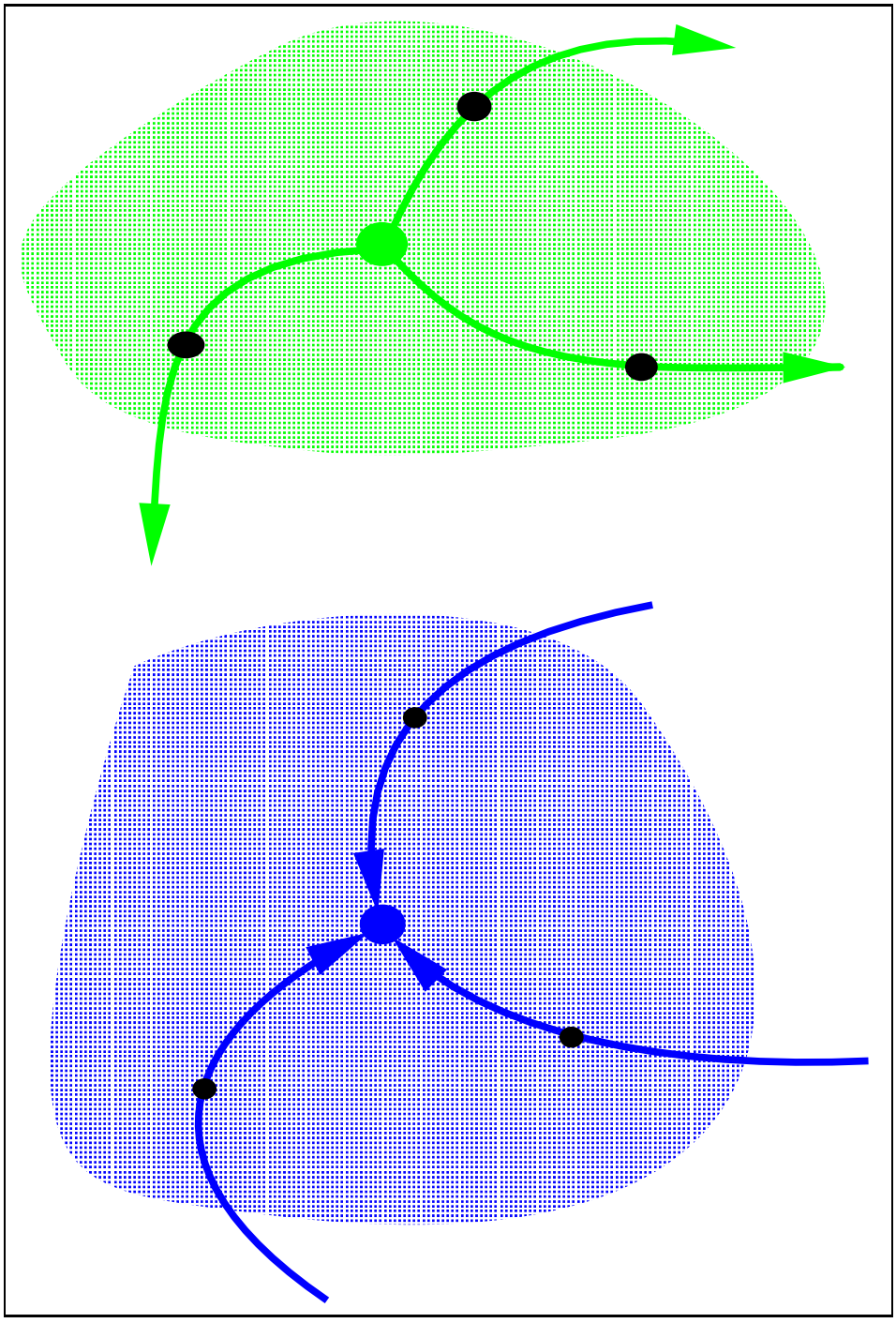

Figure 1. Around a source, every integral curve starts at the source; around a sink, every integral curve ends at the sink.

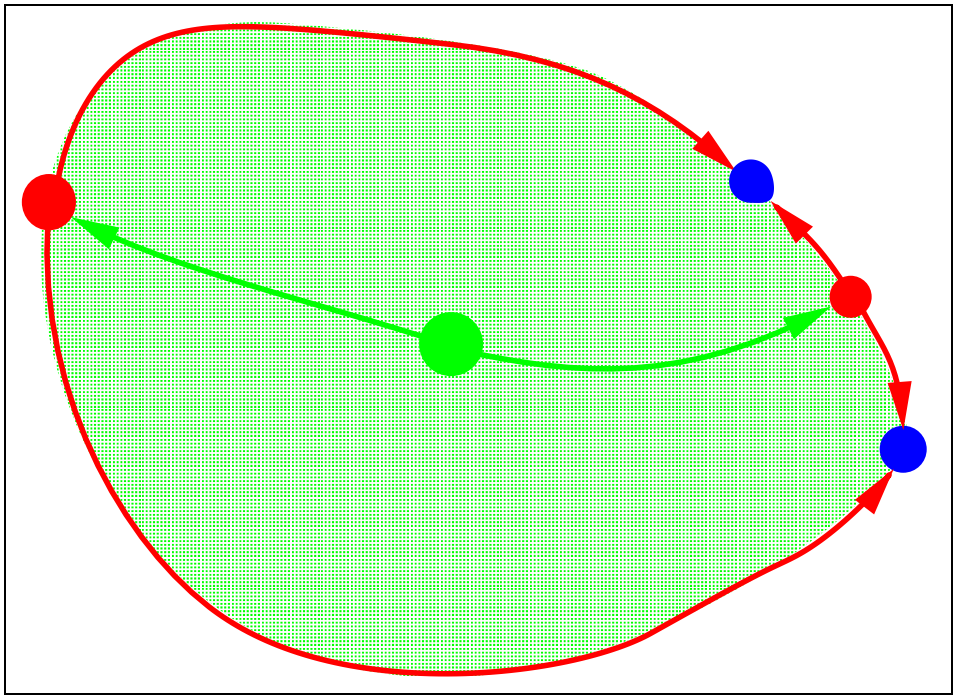

Figure 2. A typical α-basin of a source. The green basin consists of all integral curves starting at the source.

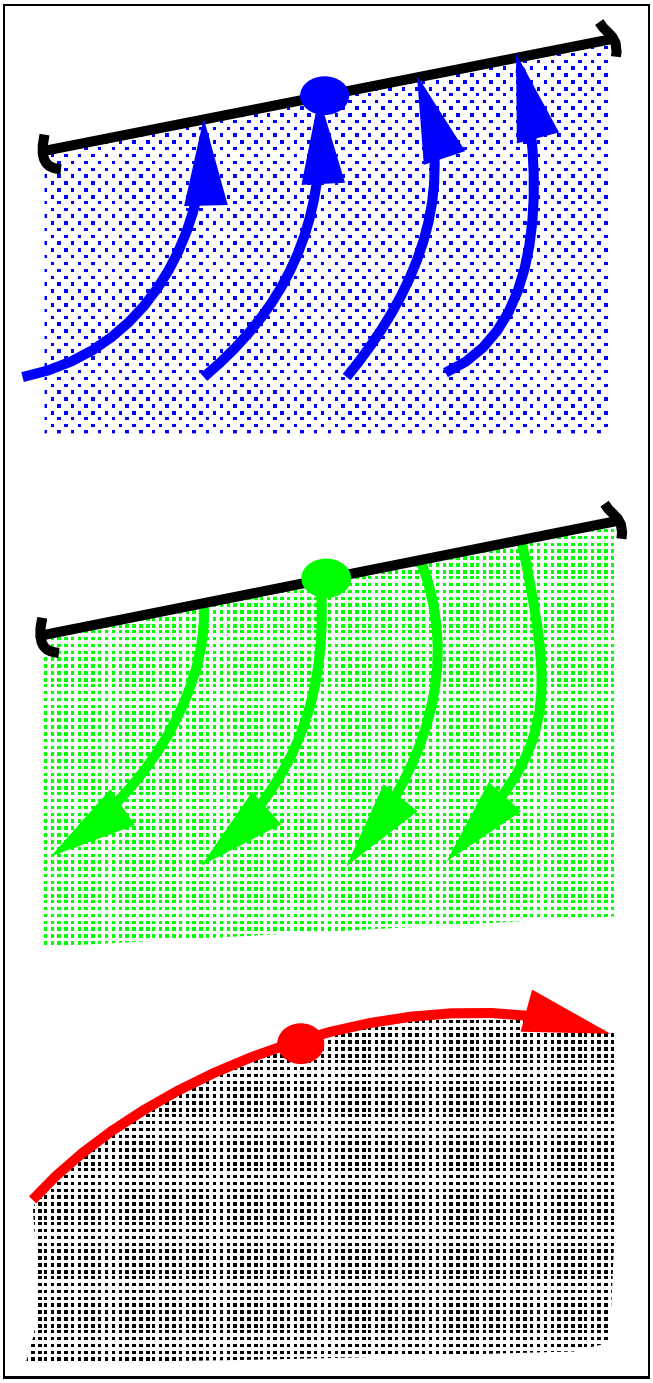

Figure 3. Around an outflow point (blue), every integral curve enters the boundary from the inside of the domain. Around a inflow point (green), every integral curve enters the inside of the domain from the boundary. At a boundary flow point (red), there exists an integral curve that stays on the boundary.

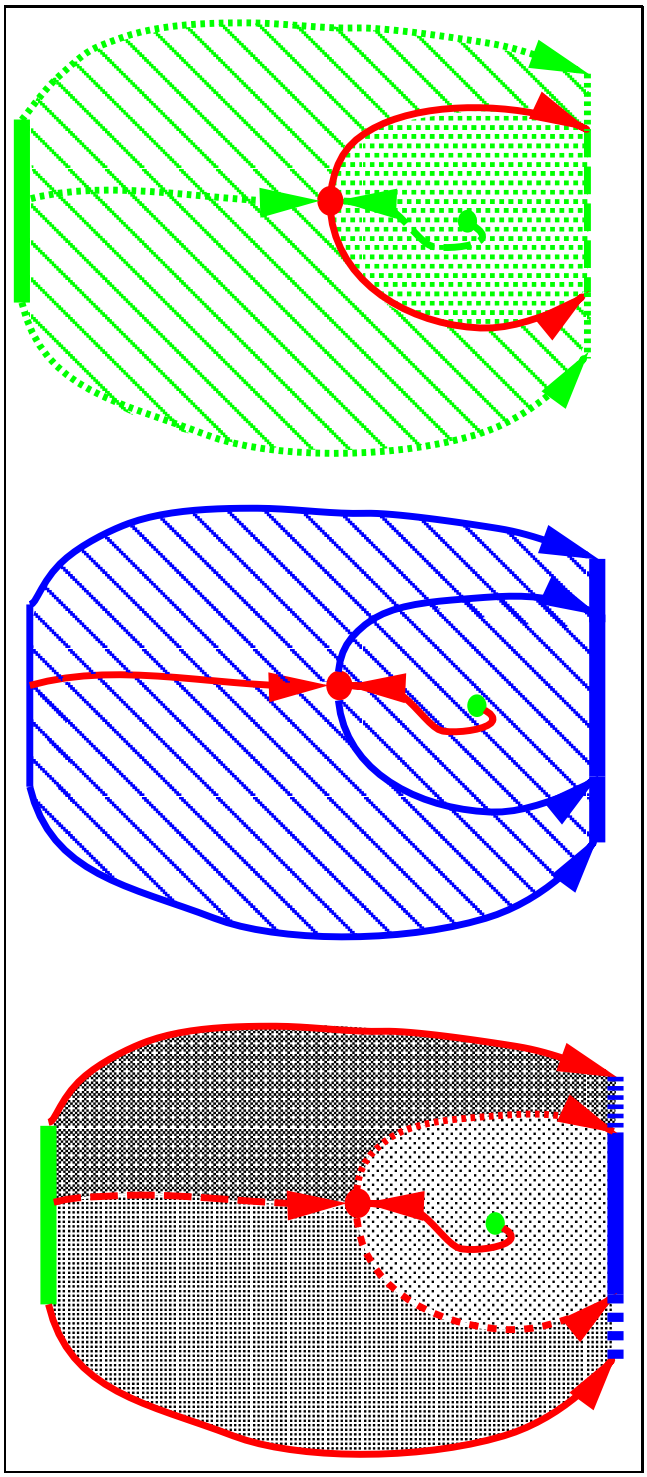

Figure 4. A simple vector field is first partioned into α-basins and then into ω-basins. The resulting different intersections of α- and ω-basins are shown in the bottom image. All α-limit sets and α-basins are colored green, all ω-limit sets and ω-basins are colored blue and the separatrices and saddles are colored red. The intersections are shown in different black patterns.

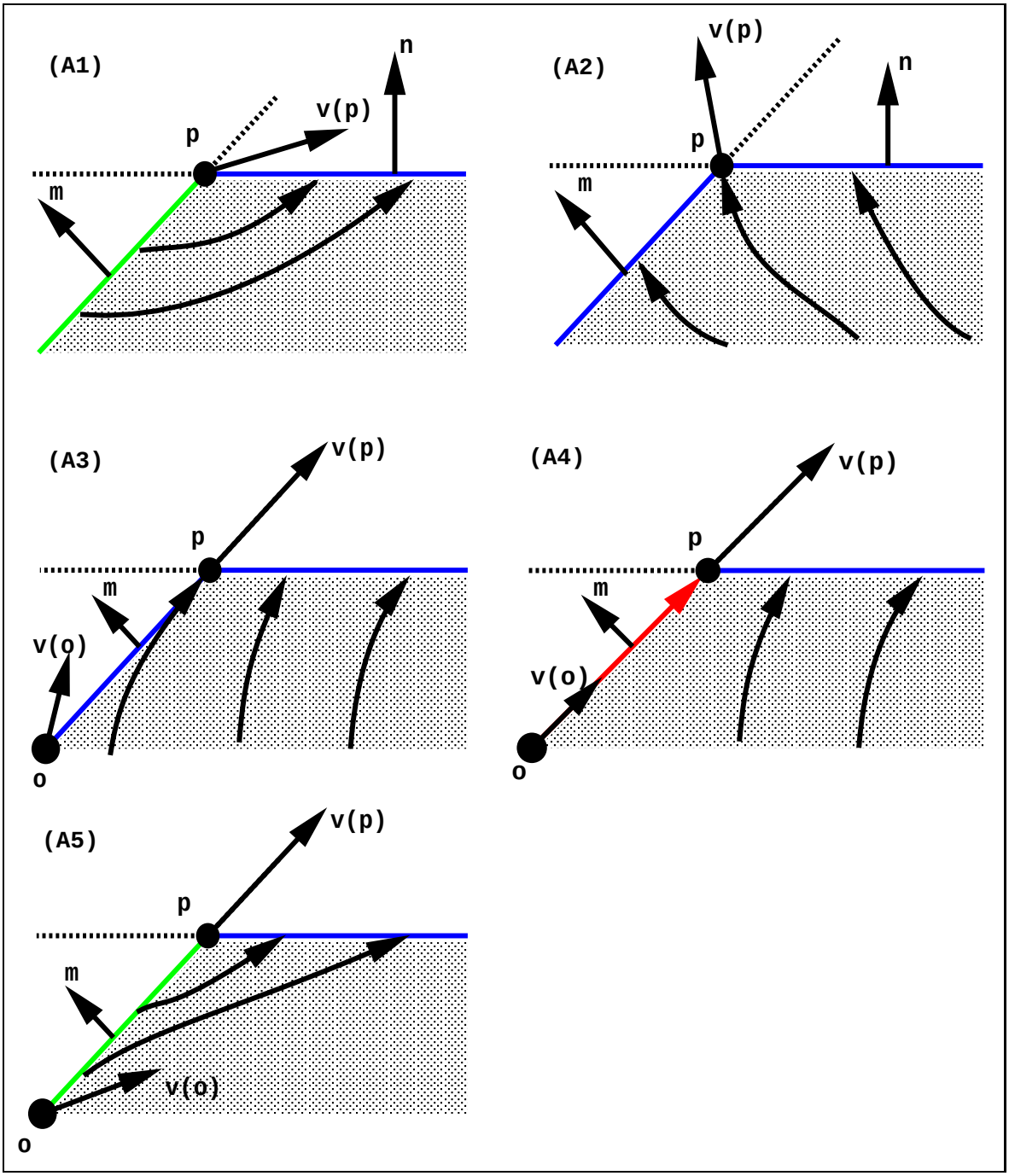

Figure 5. Convex vertex. Case (A1): inflow and outflow edges; case (A2): outflow on both edges; case (A3): flow at vertex being parallel to one edge — outflow inside both edges; case (A4): boundary flow on one edge — outflow on the other edge; case (A5): flow at vertex being parallel to one edge, inflow inside one edge, and outflow on the other edge. Inflow edges are marked green, outflow edges are marked blue, and boundary flow is marked red.

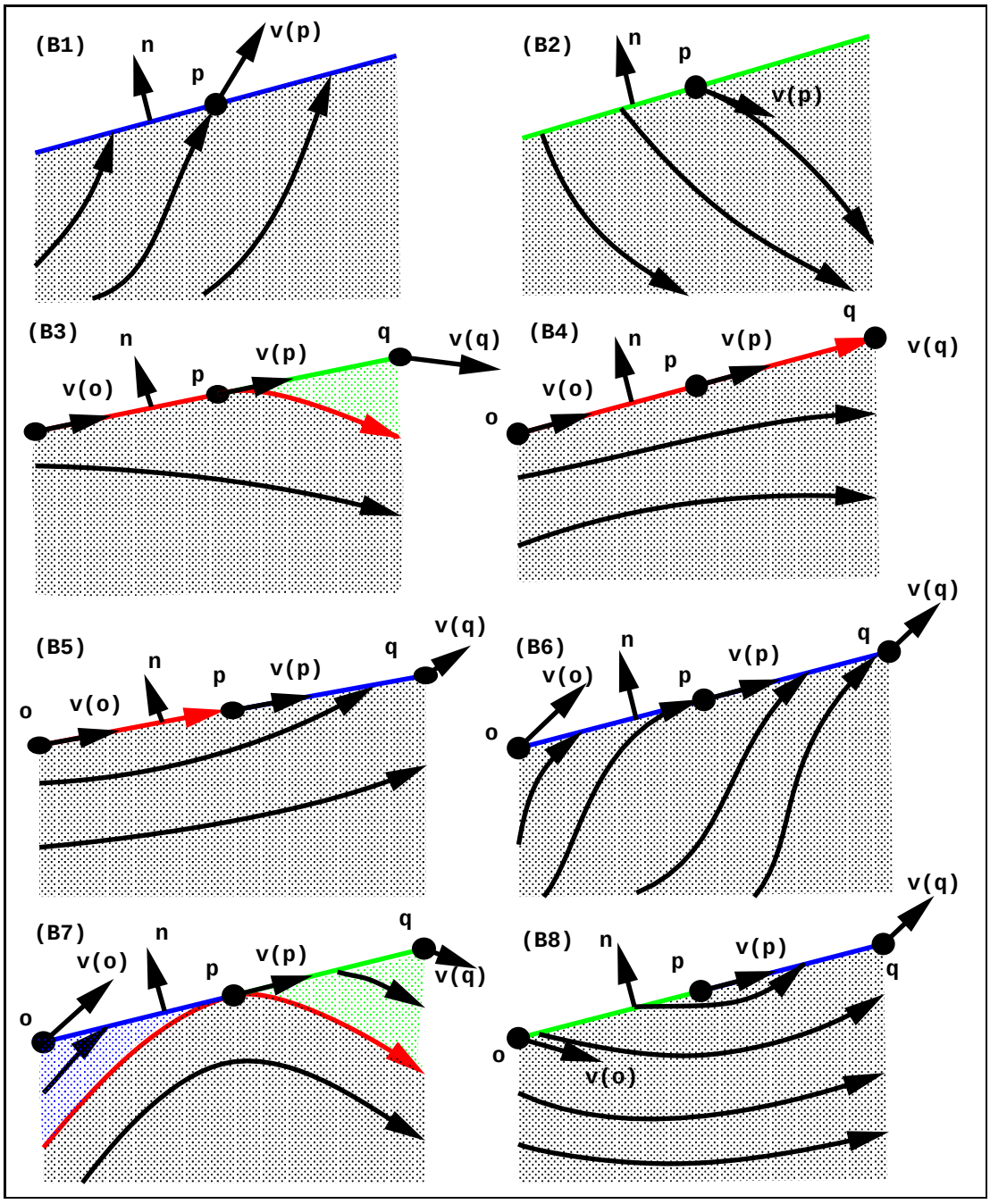

Figure 6. Collinear vertex. Case (B1): outflow at p; case (B2): inflow at p; case (B3): boundary flow on one edge and inflow on the other edge; case (B4): boundary flow on both edges; case (B5): boundary flow on one edge and outflow on the other edge; case (B6): flow parallel to the edges at p and outflow inside both edges; case (B7): flow parallel to the edges at p, inflow in the direction of the vector, and outflow on the other edge; case (B8): flow parallel to the edges at p, outflow in the direction of the vector, and inflow on the other edge. All inflow edges are colored green, outflow edges are colored blue, and boundary flow and separatrices are colored red.

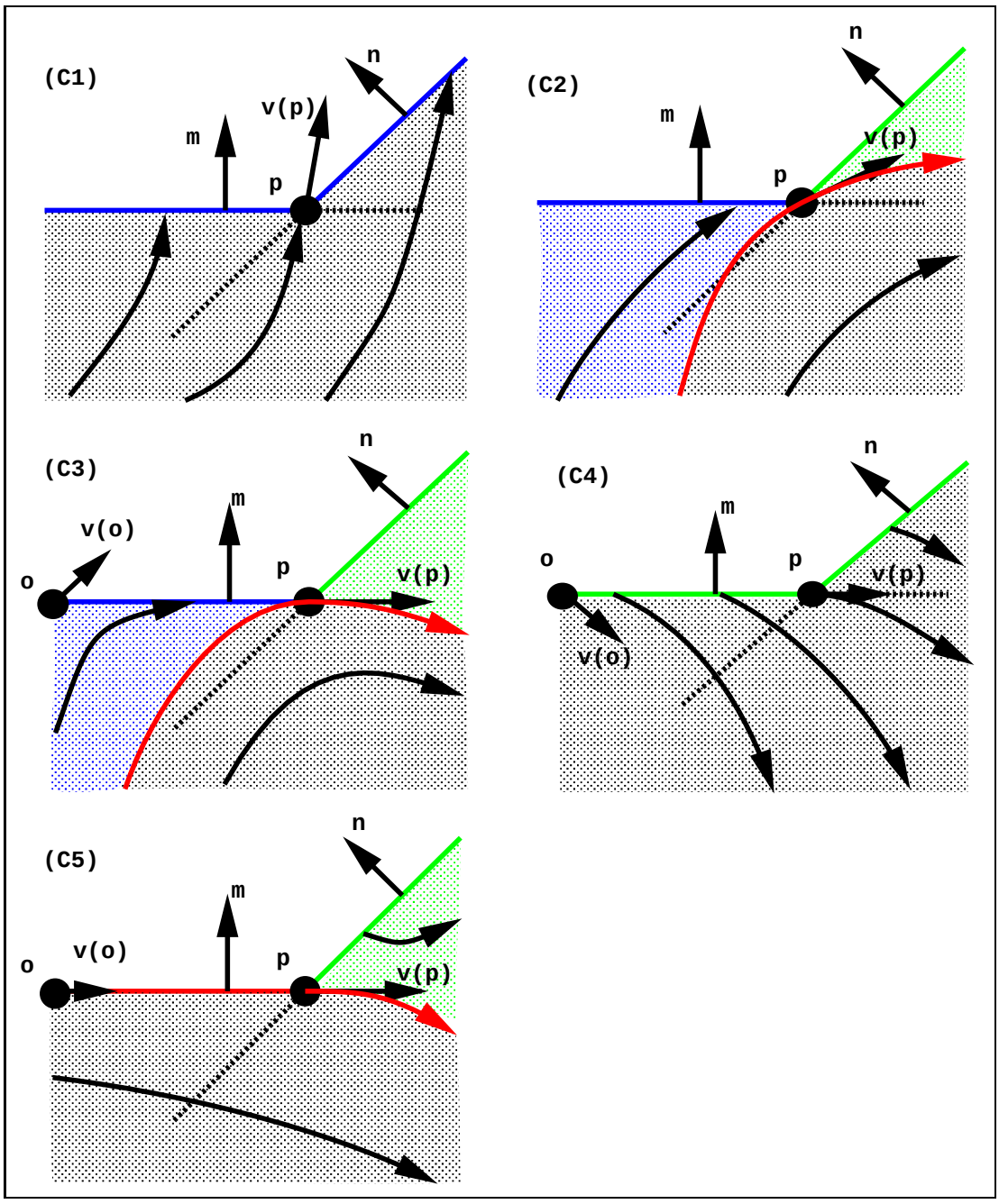

Figure 7. Concave vertex. Case (C1): outflow on both edges; case (C2): outflow on one edge and inflow on the other edge; case (C3): flow parallel to one edge at vertex p, outflow inside one edge, and inflow inside the other edge; case (C4): flow parallel to one edge at vertex p and inflow on both edges; case (C5): boundary flow on one edge and inflow on the other edge. Inflow edges and α-basins are colored green, outflow edges and ω-basins are colored blue, and separatrices and boundary flow are shown in red color.

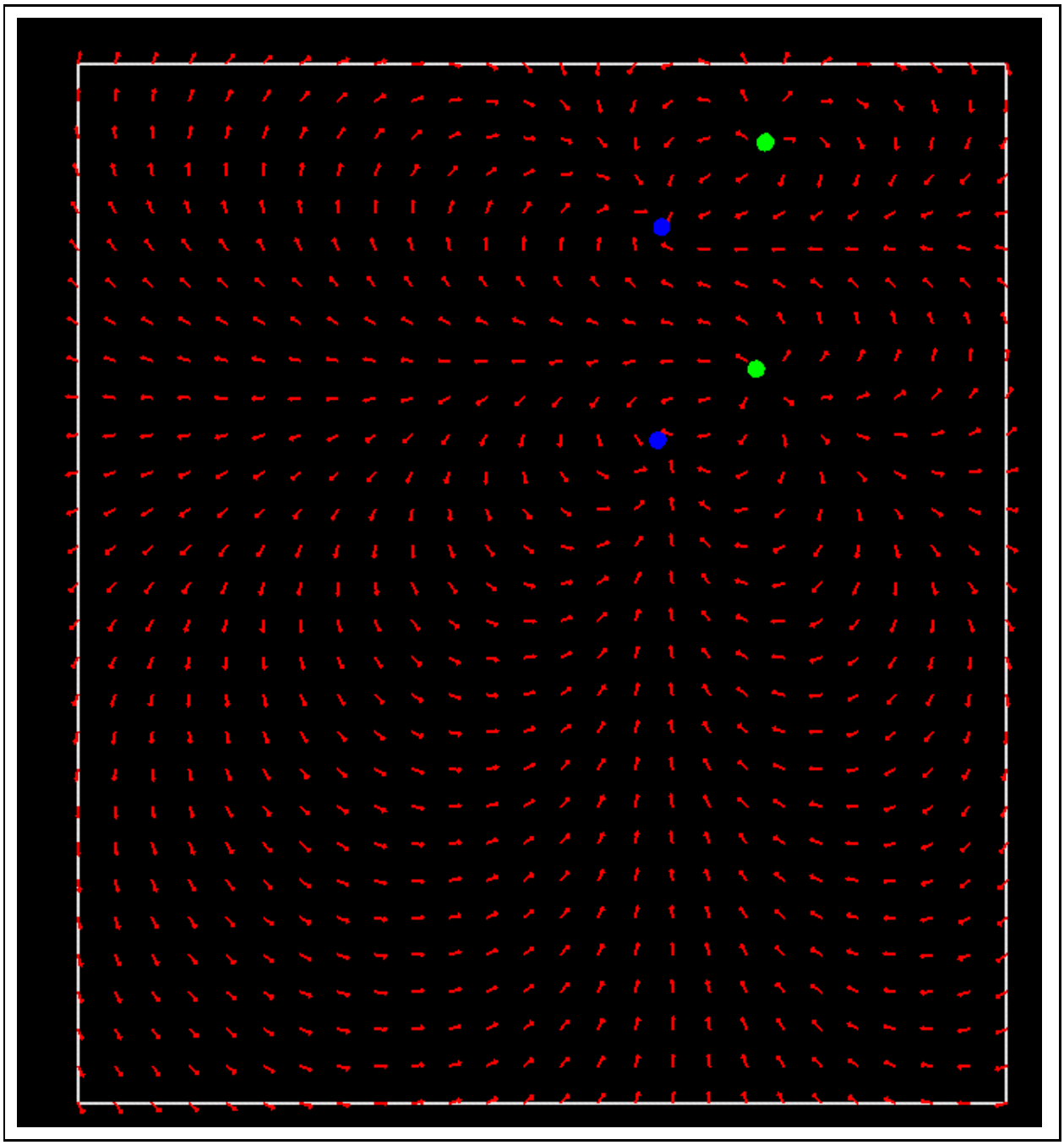

Figure 8. Vector field containing two sources and two sinks.

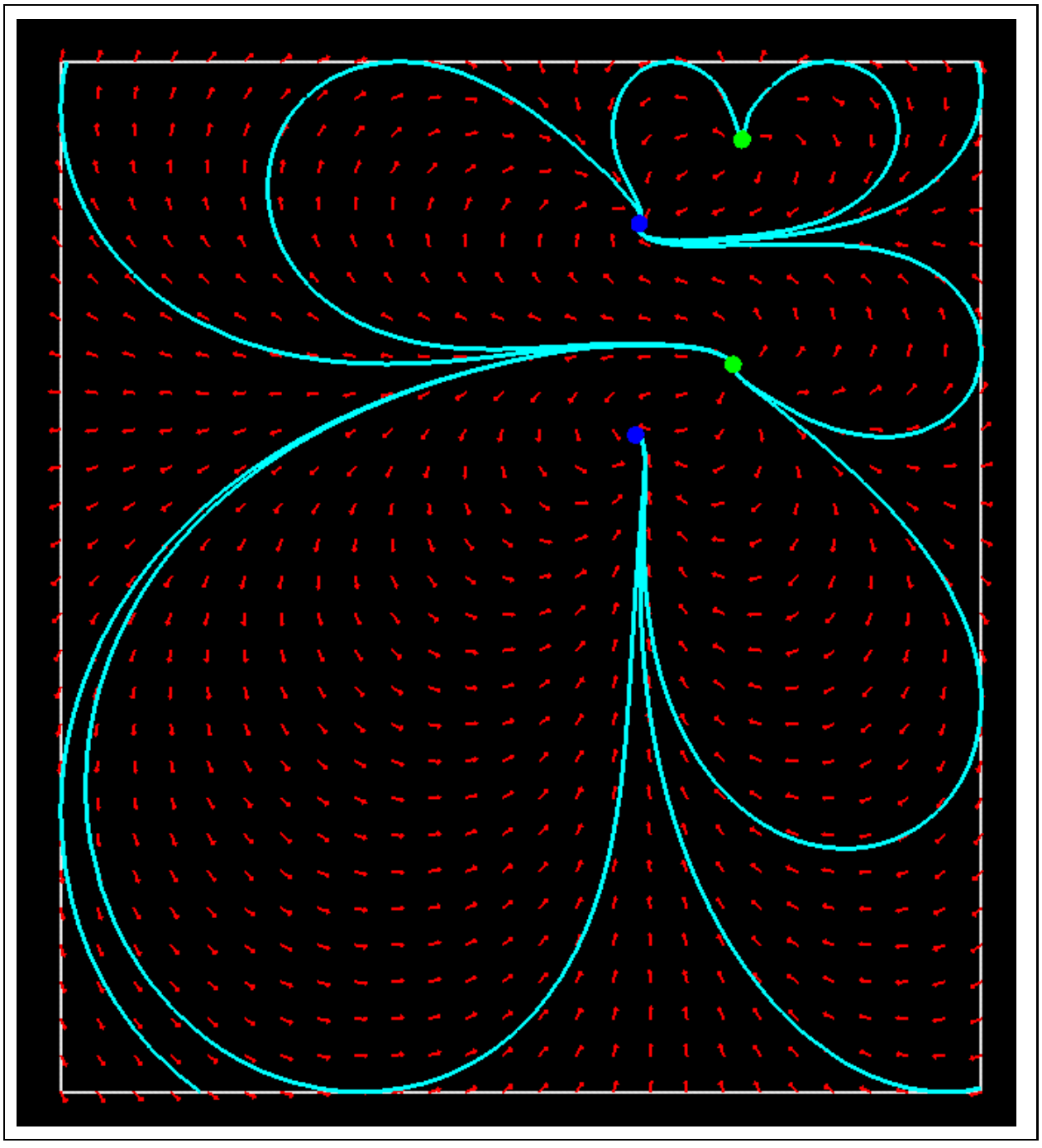

Figure 9. Local topology showing interaction of sources and sinks.

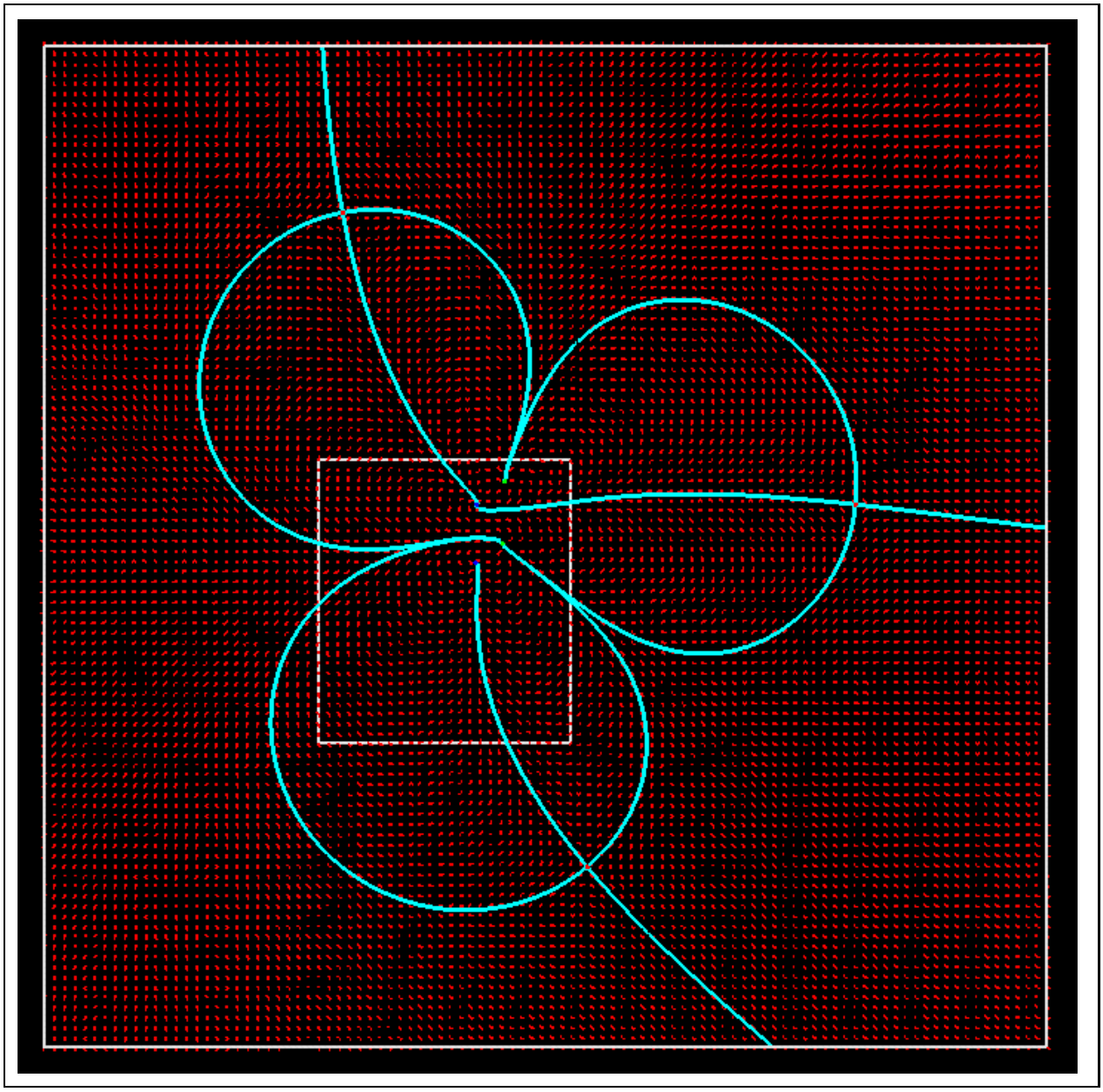

Figure 10. Global topology derived by considering entire field.

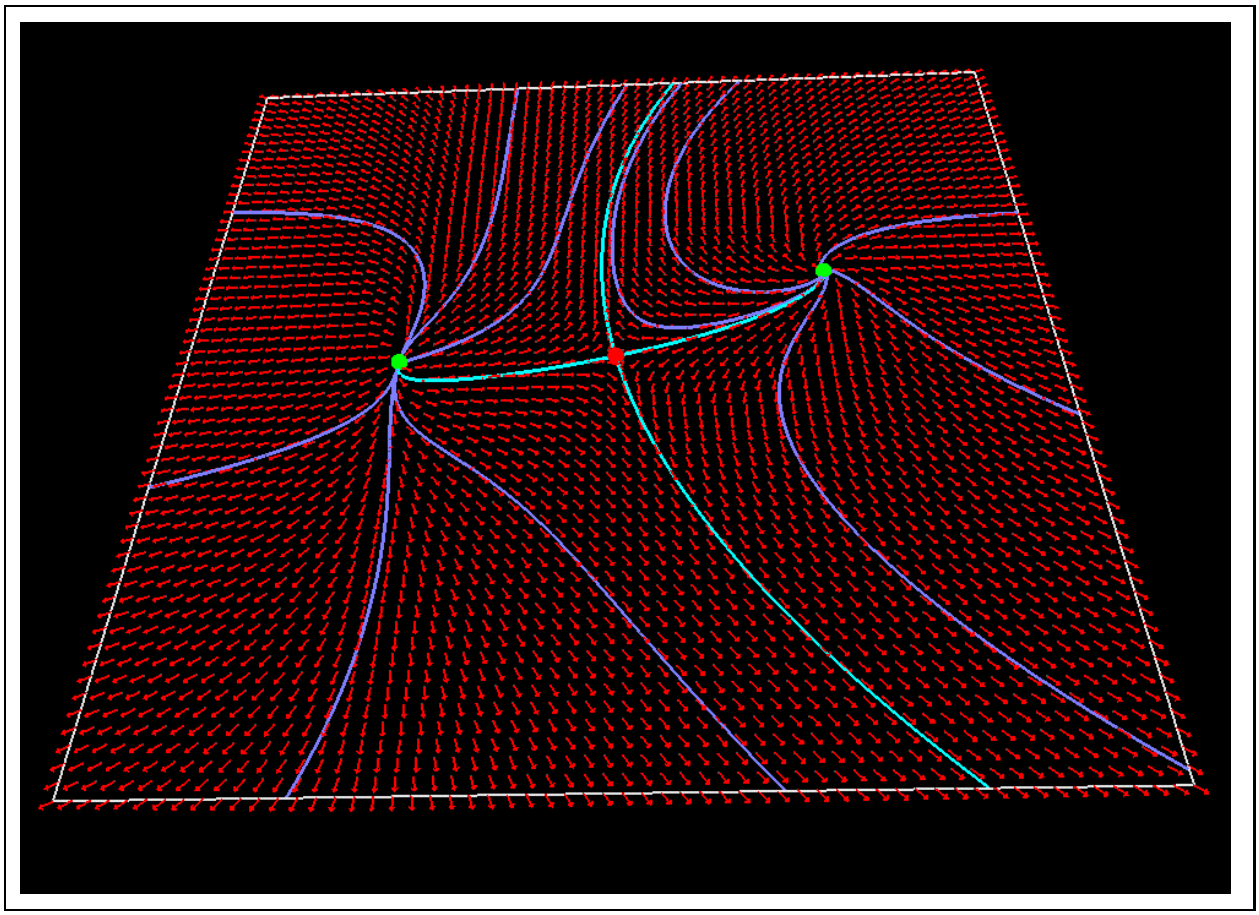

Figure 11. Analytic vector field with two sources and one saddle.

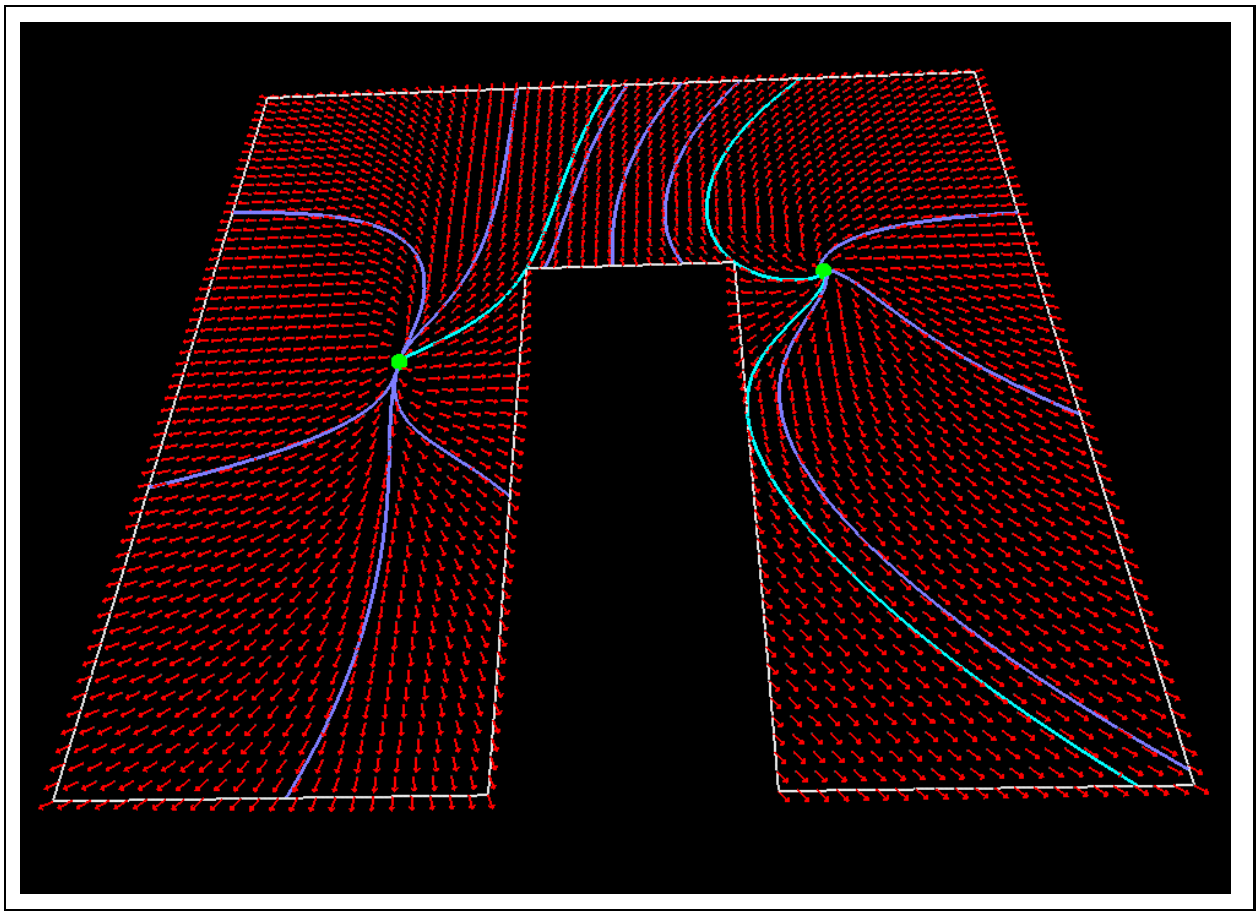

Figure 12. Local topology analysis — a rectangle containing the saddle was cut out.

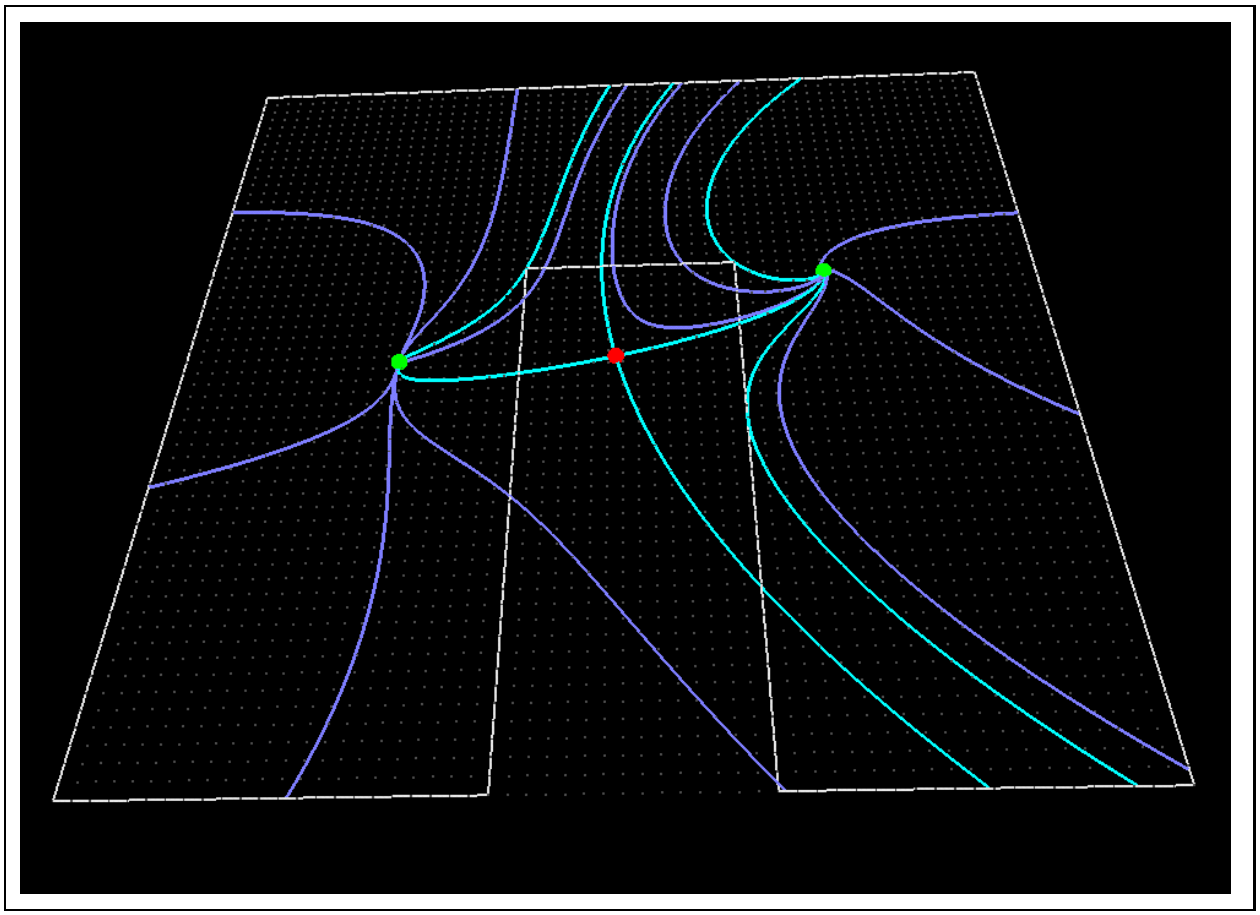

Figure 13. Comparison of results obtained with local and global topology analysis.

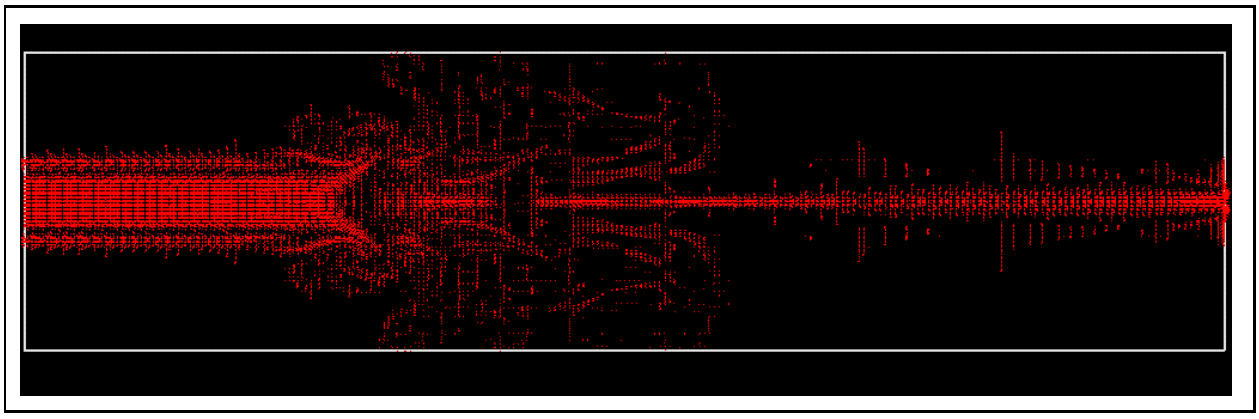

Figure 14. Turbulent jet data set.

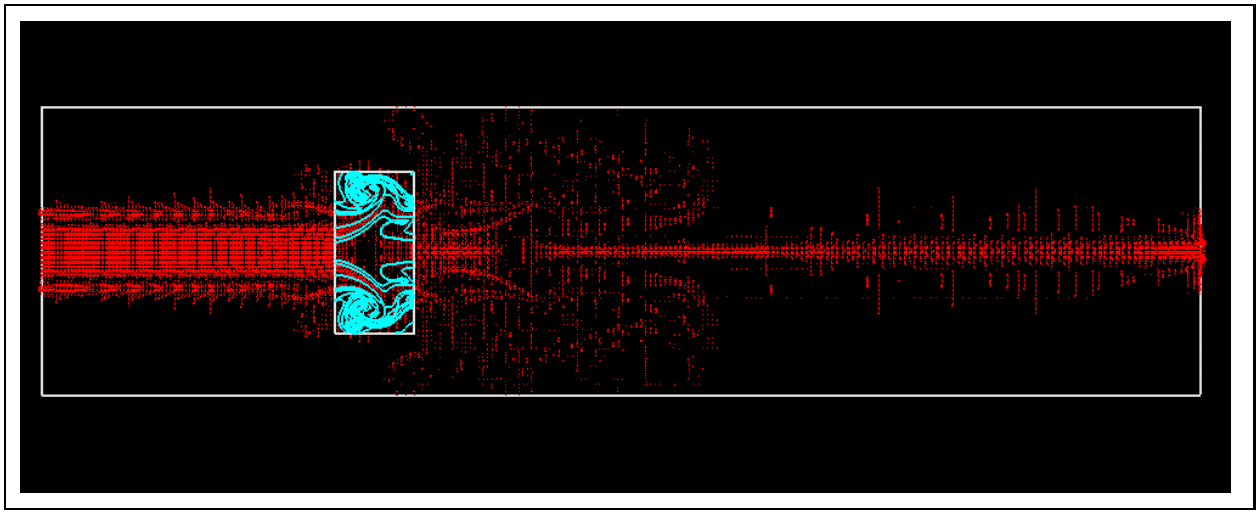

Figure 15. Rectangular region in jet data set and result of local topology analysis.

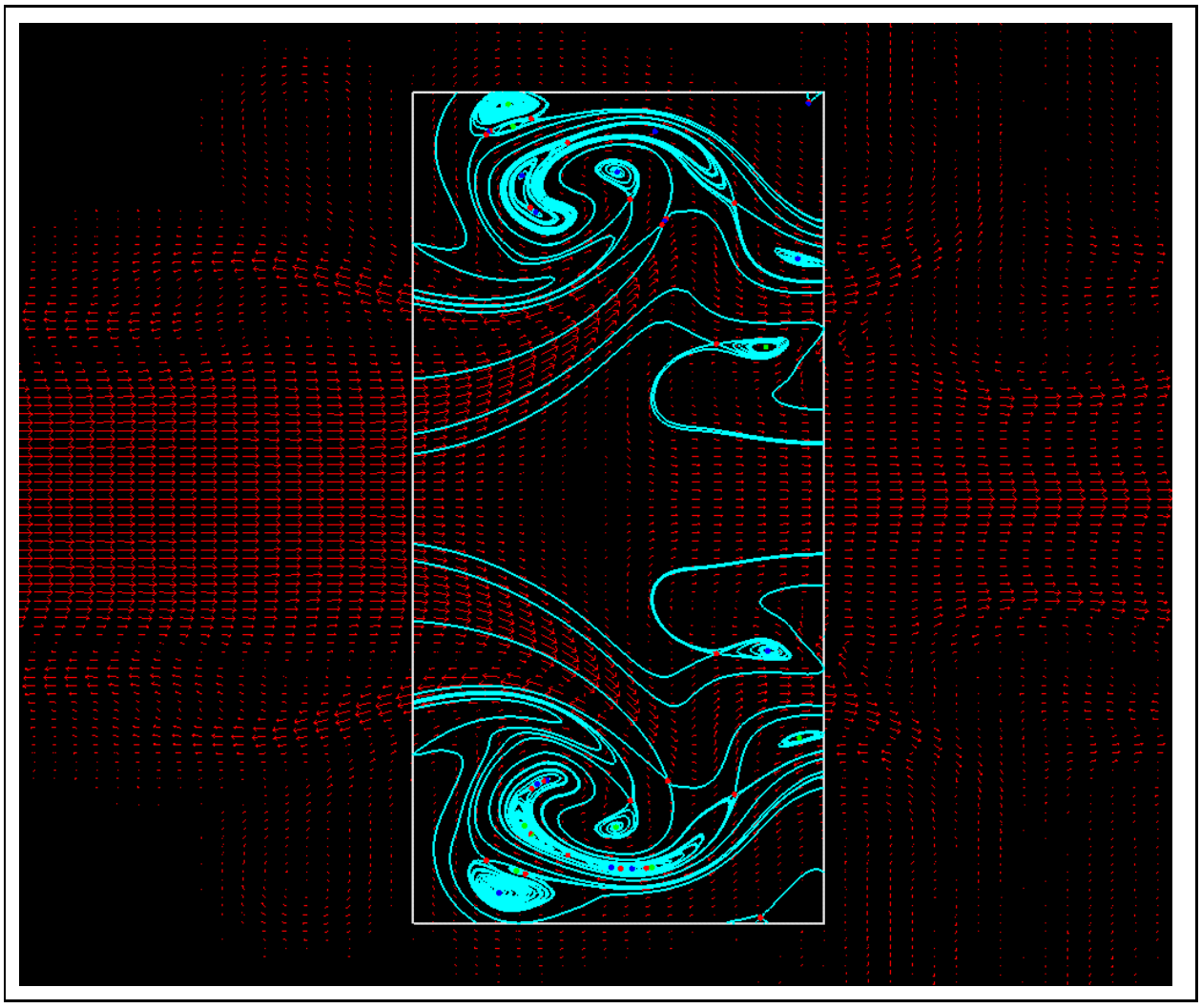

Figure 16. Magnification of result of local topology analysis shown in Figure 15.

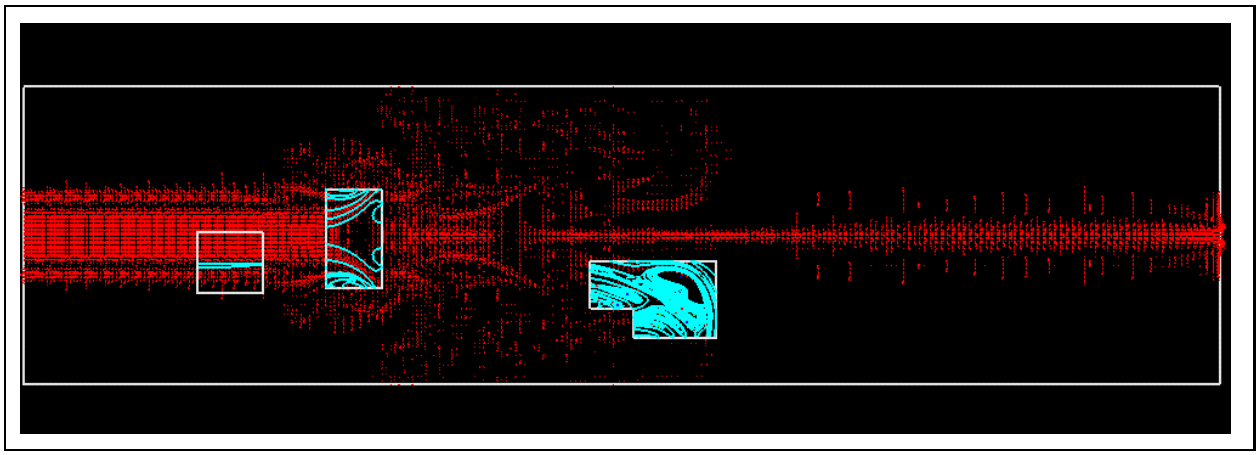

Figure 17. Three regions in jet data set and respective results of local topology analysis.

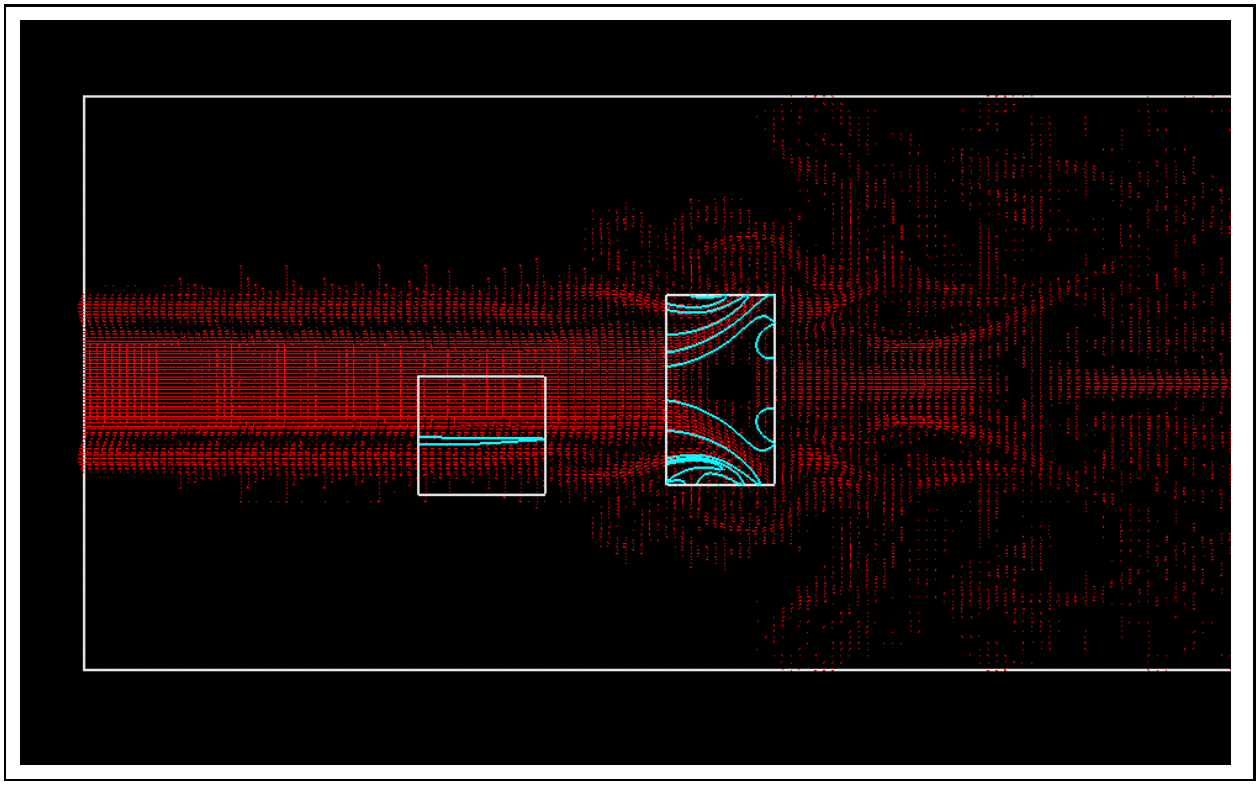

Figure 18. Local topology analysis inside two regions without critical point (jet data set).

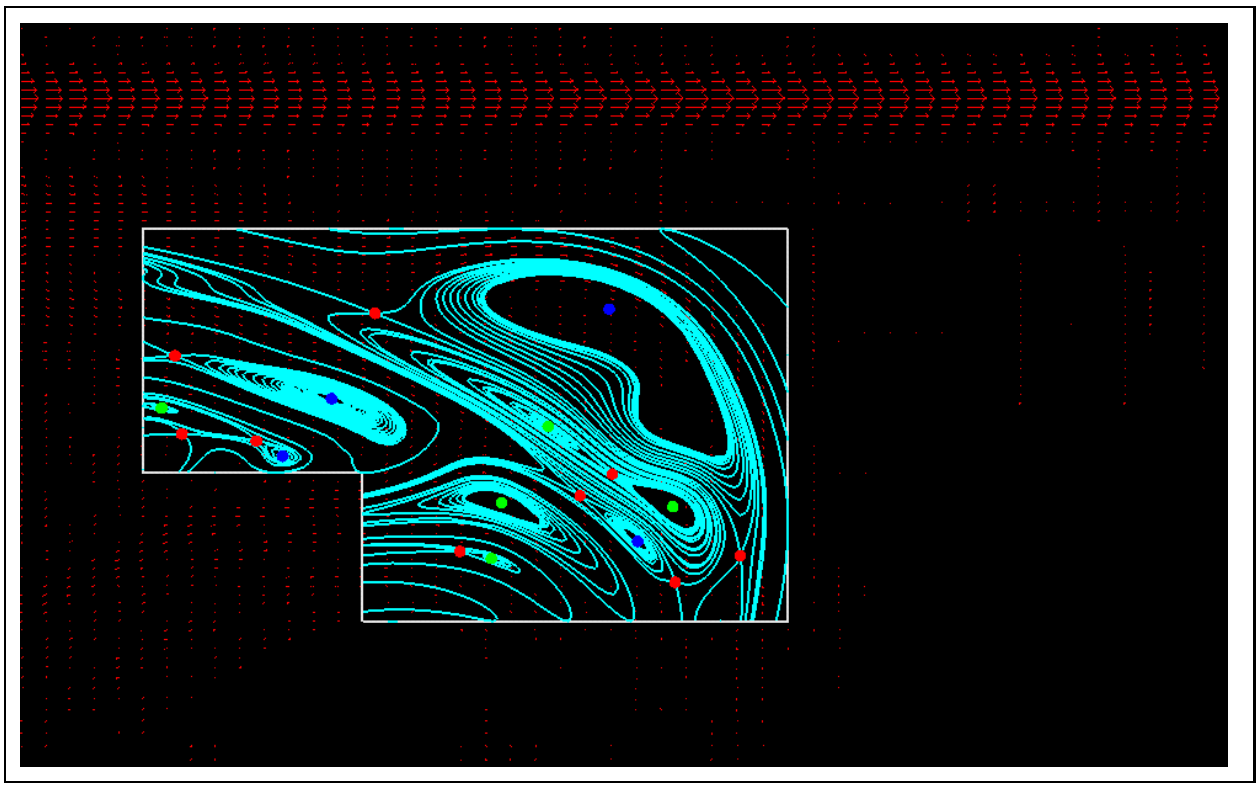

Figure 19. Local topology analysis result of highly complicated region (jet data set).

Dr. Gerik Scheuermann was born 1970 in Limburg, Germany. He received a B.S. and M.S. in mathematics in 1995 from the University of Kaiserslautern. In 1999, he received a Ph.D. in computer science, also from the University of Kaiserslautern. During 1995-1997 he conducted research at the Arizona State University for about a year. He is currently working as postdoc at the Center for Image Processing and Integrated Computing (CIPIC) at the University of California at Davis. His research topics include algebraic geometry, topology, Clifford algebra, and Scientific Visualization. Dr. Scheuermann is a member of the Institute of Electrical and Electronics Engineers (IEEE).

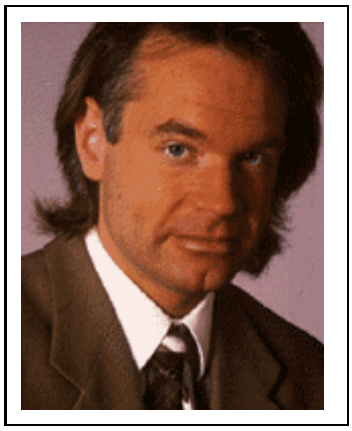

Dr. Bernd Hamann is a Full Professor of Computer Science and Co-director of the Center for Image Processing and Integrated Computing (CIPIC) at the University of California at Davis, whose faculty he joined in 1995. He is an Adjunct Professor of Computer Science at Mississippi State University, a Faculty Computer Scientist at the Lawrence Berkeley National Laboratory, and a Participating Guest researcher at the Lawrence Livermore National Laboratory. From 1991 to 1995, Dr. Hamann was a faculty member in the Department of Computer Science at Mississippi State University, where he was

also affiliated with the NSF Engineering Research Center for Computational Field Simulation. His primary interests are visualization, computer-aided geometric design, computer graphics, and virtual reality, with a focus on hierarchical approximation visualization methods. Dr. Hamann serves on the Editorial Board of the IEEE Transactions on Visualization and Computer Graphics and served as a Papers Co-chair/Proceedings Co-editor for the IEEE Visualization conferences in 1999 and 2000. He is the author or co-author of over 80 peer-reviewed publications and has given invited presentations at leading conferences and institutions in the U.S. and in Europe.

Dr. Hamann received a B.S. in computer science, a B.S. in mathematics, and an M.S. in computer science from the Technical University of Braunschweig, Germany. He received a Ph.D. in computer science from Arizona State University in 1991 under the supervision of Dr. Gregory M. Nielson. Dr. Hamann was awarded a 1992 Research Initiation Award by Mississippi State University, a 1992 Research Initiation Award by the National Science Foundation, and a 1996 CAREER Award by the National Science Foundation. In 1995, he received a Hearin-Hess Distinguished Professorship in Engineering by the College of Engineering at Mississippi State University. Dr. Hamann is a member of the Association for Computing Machinery (ACM), the Institute of Electrical and Electronics Engineers (IEEE), the Society for Industrial and Applied Mathematics (SIAM), and the IEEE Technical Committee on Visualization and Graphics (TCVG).

Dr. Kenneth I. Joy is a Full Professor of Computer Science at the University of California at Davis. He came to UC Davis in 1980 in the Department of Mathematics and was a founding member of the Computer Science Department in 1983. His primary interests are visualization, geometric modeling and computer graphics.

Joy received a B.A. and M.A. in mathematics from UCLA, and a Ph.D in mathematics from the University of Colorado in 1976. He is a member of the Association for Computing Machinery (ACM), the Institute of Electrical and Electronics Engineers (IEEE), and the Society for Industrial and Applied Mathematics (SIAM).

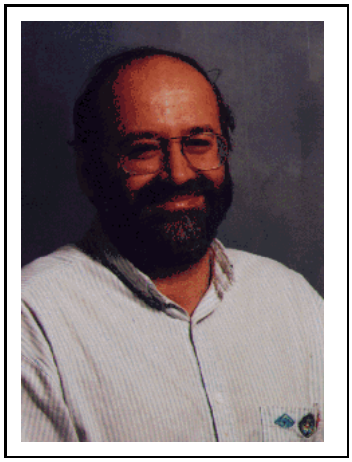

Dr. Wolfgang Kollmann is a full professor in the Mechanical and Aeronautical Engineering Department of the University of California at Davis. He joined the department in 1981. His research interests are turbulence, turbulent combustion and the numerical simulation of turbulent flows. He is member of APS, AIAA, SIAM. He graduated from the University of Stuttgart, Germany, in Aeronautical Engineering in 1969 and received his PhD in Mechanical Engineering from the Technical University Aachen, Germany in 1973.